

A SPECTRAL MIMETIC LEAST-SQUARES METHOD

PAVEL BOCHEV AND MARC GERRITSMAN

Abstract We present a spectral mimetic least-squares method for a model diffusion-reaction problem, which preserves key conservation properties of the continuum problem. Casting the model problem into a first-order system for two scalar and two vector variables shifts material properties from the differential equations to a pair of constitutive relations. We use this system to motivate a new least-squares functional involving all four fields and show that its minimizer satisfies the differential equations exactly. Discretization of the four-field least-squares functional by spectral spaces compatible with the differential operators leads to a least-squares method in which the differential equations are also satisfied exactly. Moreover, the latter are reduced to purely topological relationships for the degrees of freedom that can be satisfied without reference to basis functions. Numerical experiments confirm the spectral accuracy of the method and its local conservation.

CONTENTS

1. Introduction	2
2. The model problem deconstructed	3
2.1. A mimetic least-squares method	5
3. Topological discretizations of the differential equations	7
3.1. Basic concepts from algebraic topology	7
3.2. Mimetic approach for the differential equations	8
4. Spectral basis functions	10
4.1. One-dimensional spectral basis functions	11
4.2. Two-dimensional 0-cochain and 1-cochain spectral basis functions	14
4.3. Two-dimensional 2-cochain and 3-cochain spectral basis functions	15
5. Discretization of the constitutive relations	17
6. Transformation of discrete approximations	18
7. Results	20
7.1. Least-squares and mimetic least-squares functional	21
7.2. Different polynomial representations on dual elements	23
7.3. Mimetic least-squares on deformed grids	26
8. Conclusions	28
References	29

Date: March 6, 2014.

1991 Mathematics Subject Classification. Primary 65N30, 65N35; Secondary 35J20, 35J46.

Key words and phrases. Least-squares, mimetic methods, algebraic topology, spectral elements, geometric localization.

This paper is in final form and no version of it will be submitted for publication elsewhere.

1. INTRODUCTION

We consider the model diffusion-reaction problem

$$(1) \quad \begin{aligned} -\nabla \cdot \mathbb{A} \nabla \phi + \gamma \phi &= f & \text{in } \Omega, \\ \phi &= g & \text{on } \Gamma_D, \\ \mathbf{n} \cdot \mathbb{A} \nabla \phi &= h & \text{on } \Gamma_N, \end{aligned}$$

where $\Omega \subset \mathbb{R}^n$ has a Lipschitz-continuous boundary $\partial\Omega = \Gamma_D \cup \Gamma_N$ and \mathbf{n} is the outward unit normal to $\partial\Omega$. We assume that \mathbb{A} is a symmetric positive definite tensor and γ is a real-valued, strictly positive function, i.e., there exist constants $f_{min}, f_{max}, \gamma_{min}, \gamma_{max} > 0$ such that

$$(2) \quad f_{min} \boldsymbol{\xi}^T \boldsymbol{\xi} \leq \boldsymbol{\xi}^T \mathbb{A}(\mathbf{x}) \boldsymbol{\xi} \leq f_{max} \boldsymbol{\xi}^T \boldsymbol{\xi} \quad \text{and} \quad \gamma_{min} \leq \gamma(\mathbf{x}) \leq \gamma_{max},$$

for all $\mathbf{x} \in \Omega$ and $\boldsymbol{\xi} \in T_{\mathbf{x}}\Omega$. The tensor \mathbb{A} and the function γ describe material properties. For instance, in heat transfer applications \mathbb{A} is the thermal conductivity of the material and γ can be related to the specific heat capacity.

Almost all published¹ least-squares methods for (1) start with the reformulation of the governing equations into an equivalent first-order system

$$(3) \quad \begin{aligned} \nabla \cdot \mathbf{u} + \gamma \phi &= f & \text{in } \Omega, \\ \mathbf{u} + \mathbb{A} \nabla \phi &= 0 & \text{in } \Omega, \\ \phi &= g & \text{on } \Gamma_D, \\ \mathbf{n} \cdot \mathbf{u} &= -h & \text{on } \Gamma_N. \end{aligned}$$

followed by setting up a least-squares functional

$$(4) \quad \mathcal{J}(\mathbf{u}, \phi; f) := \frac{1}{2} \left(\|\nabla \cdot \mathbf{u} + \gamma \phi - f\|_X^2 + \|\mathbf{u} + \mathbb{A} \nabla \phi\|_Y^2 \right),$$

and a least-squares principle, which is the following unconstrained minimization problem:

$$(5) \quad (\mathbf{u}, \phi) = \arg \min_{\mathbf{v} \in U, \varphi \in V} \mathcal{J}(\mathbf{v}, \varphi; f).$$

We will refer to ϕ and \mathbf{u} as the *potential* and *flux* variables. In (4)–(5) X, Y and U, V are some appropriate *data* and *solution* spaces. The key juncture in the definition of a well-posed least-squares method is to choose these spaces such that \mathcal{J} is norm-equivalent, i.e., the residual “energy” $\|(\mathbf{u}, \phi)\| := \mathcal{J}(\mathbf{u}, \phi; 0)$ defines an equivalent norm on the solution spaces:

$$(6) \quad C_1 \left(\|\mathbf{v}\|_U^2 + \|\varphi\|_V^2 \right) \leq \|(\mathbf{v}, \varphi)\|^2 \leq C_2 \left(\|\mathbf{v}\|_U^2 + \|\varphi\|_V^2 \right), \quad \forall \mathbf{v} \in U, \varphi \in V.$$

This guarantees the strong coercivity of the Euler-Lagrange equation for (5), which is the least-squares variational problem. As a result, restriction of the least-squares principle (5) to finite dimensional subspaces $U^h \subset U$ and $V^h \subset V$ yields a well-posed discrete least-squares problem with symmetric and positive definite linear system. This obviates the need for an inf-sup condition and makes the method amenable to well-established iterative solvers, which is one of the key advantages of least-squares methods. Furthermore, norm-equivalence (6) implies that minimization of \mathcal{J} amounts to minimization of the error in \mathbf{u} and ϕ in their respective norms. Therefore, the least-squares functional provides a natural a posteriori error estimator [9], which is another important advantage of least-squares methods.

One common choice for which (6) holds is $X = Y = L^2(\Omega)$, $U = H(\text{div}, \Omega)$ and $V = H^1(\Omega)$. Because strong coercivity is inherited on subspaces, one can approximate both

¹The negative norm least-squares method for second order elliptic equations [7] is one notable exception.

solution spaces by standard C^0 elements. Since the inception of least-squares methods this has often been quoted as one of their principal advantages. However, when formulated in this way, the least-squares method is not conservative [14, 15, 25] and in some cases solutions can be very inaccurate; see [3, 10] for examples.

The use of div-conforming elements for the flux, such as Raviart-Thomas elements [27], has been suggested in [2] as a way to improve the accuracy and conservation of least-squares methods for (1). Analysis in [2] shows that div-conforming elements enable optimal L^2 convergence of the flux, which does not hold true for nodal elements. Furthermore, the flux approximation becomes locally conservative.

In this paper we extend these ideas to develop a *spectral* mimetic least-squares method for (1) that is locally conservative. Reformulation of the model problem into a *four-field* first-order system involving two scalar and two vector variables allows us to shift material parameters from the differential operators into a pair of constitutive relations. The four-field system prompts the inclusion of two new equation residuals to the standard least-squares formulation (4). We show that the resulting least-squares principle satisfies exactly the differential equations, while the constitutive relations are satisfied approximately. The key idea then is to approximate the four fields by finite elements from a discrete exact sequence. This allows us to satisfy exactly the differential equations in the discrete setting and yields a locally conservative least-squares method.

In contrast to other high-order methods, which utilize modal degrees of freedom, our approach uses compatible spectral elements with geometrically localized degrees of freedom; see, e.g., [26] for a related construction of high-order Whitney elements on simplices. Because these degrees of freedom live on geometric mesh entities, they are co-chains of the same order as the dimension of the entity. This reduces the action of differential operators such as div, grad and curl to the action of the co-boundary operator on the corresponding co-chain, i.e., the discretized differential operators are purely topological and independent of the size or shape of the mesh. As a result, our approach transforms the differential equations into purely topological relationships for the degrees of freedom that can be satisfied without reference to basis functions. In so doing we obtain a least-squares method in which the discrete differential equations are satisfied exactly, and the approximation takes place in the constitutive relations involving \mathbb{A} and γ .

The rest of the paper is organized as follows. Section 2 transforms (1) into a first-order four field system and explains the formulation of the mimetic least-squares method. Section 3 derives topological discretizations of the differential equations, which are independent of the basis functions. Section 4 presents the corresponding compatible spectral elements used in this work. We discuss approximation of constitutive laws, which depends on the basis functions, in Section 5. In Section 6 the behavior under mappings will be presented. We conclude with numerical examples in Section 7 and conclusions in Section 8.

2. THE MODEL PROBLEM DECONSTRUCTED

Our starting point is the following least-squares principle for the first-order system (3):

$$(7) \quad \min_{\phi \in U, \mathbf{u} \in V} \mathcal{J}(\phi, \mathbf{u}) := \frac{1}{2} \left(\|\mathbb{A}^{-1/2} (\mathbf{u} + \mathbb{A} \nabla \phi)\|_0^2 + \|\gamma^{-1/2} (\gamma \phi + \nabla \cdot \mathbf{u} - f)\|_0^2 \right).$$

To motivate the mimetic least-squares method we reformulate (1) into an equivalent first-order system involving two scalar and two vector variables. To this end, we introduce two more variables defined by

$$(8) \quad \mathbf{v} = \mathbb{A}^{-1} \mathbf{u} \quad \text{and} \quad \psi = \gamma \phi,$$

respectively. Then, the model problem (1) can be written as

$$(9) \quad \begin{aligned} \nabla \cdot \mathbf{u} + \psi &= f & \text{in } \Omega, & \quad \mathbf{v} = \mathbb{A}^{-1} \mathbf{u} & \text{in } \Omega, & \quad \text{and} & \quad \phi = g & \text{on } \Gamma_D, \\ \mathbf{v} + \nabla \phi &= 0 & \text{in } \Omega, & \quad \psi = \gamma \phi & \text{in } \Omega, & \quad \text{and} & \quad -\mathbf{n} \cdot \mathbf{u} = h & \text{on } \Gamma_N. \end{aligned}$$

As a result of these substitutions, the first two equations

$$(10) \quad \nabla \cdot \mathbf{u} + \psi = f \quad \text{and} \quad \mathbf{v} + \nabla \phi = 0,$$

have become independent of the material properties \mathbb{A} and γ . The first equation expresses a conservation law, which can be directly related to the fluxes $\mathbf{u} \cdot \mathbf{n}$ over the boundary of a volume and the second equation expresses the fact that $\nabla \times \mathbf{v} \equiv 0$. These two conservation laws provide a *complementary view* of the same physical process. Loosely speaking, the divergence relation describes this process using a normal component of velocity flux *through* a surface, whereas the gradient relation describes the same process by using a tangential component of the velocity *along* a curve. In the discrete world the two view points generally *cannot coexist on the same grid*, i.e. the vector variable can be a *flux* or a *velocity*, but *not both*.

The two new equations, (8), are constitutive laws involving the material parameters. Note that these laws do *not* involve derivatives. By introducing \mathbf{v} as a new variable, we have \mathbf{u} for the flux and \mathbf{v} for the velocity which allows for an independent discrete representation.

The two differential equations, $\nabla \cdot \mathbf{u} + \psi = f$ and $\mathbf{v} + \nabla \phi = 0$, only depend on the space topology and, in the discrete setting, on the grid topology. This property is employed in mimetic methods to exactly represent these equations without any reference to the size and shape of the grid, [5, 17, 18, 19, 22, 28].

Motivated by these properties of mimetic methods we define a new least-squares functional by augmenting (7) with the residuals of the ‘‘topological’’ equations (10)

$$(11) \quad \begin{aligned} \mathcal{J}((\phi, \mathbf{v}), (\psi, \mathbf{u}); f) &= \\ &= \frac{1}{2} \left(\|\mathbb{A}^{-1/2}(\mathbf{u} + \mathbb{A} \nabla \phi)\|_0^2 + \|\gamma^{-1/2}(\gamma \phi + \nabla \cdot \mathbf{u} - f)\|_0^2 + \|\mathbf{v} + \nabla \phi\|_0^2 + \|\nabla \cdot \mathbf{u} + \psi - f\|_0^2 \right), \end{aligned}$$

and consider the associated least-squares principle

$$(12) \quad \min_{(\phi, \mathbf{v}) \in U, (\psi, \mathbf{u}) \in V} \mathcal{J}((\phi, \mathbf{v}), (\psi, \mathbf{u}); f)$$

where $U = H^1(\Omega) \times (L^2(\Omega))^n$ and $V = L^2(\Omega) \times H(\text{div}, \Omega)$.

Our first result shows that (12) is a well-posed minimization problem.

Theorem 1. *For homogeneous boundary conditions, $g = h = 0$, the least-squares functional $\mathcal{J}((\phi, \mathbf{v}), (\psi, \mathbf{u}); 0)$ is norm-equivalent:*

$$(13) \quad \mathcal{J}((\phi, \mathbf{v}), (\psi, \mathbf{u}); 0) \sim \|\mathbf{u}\|_{H(\text{div}, \Omega)} + \|\phi\|_{H^1(\Omega)} + \|\mathbf{v}\|_{L^2(\Omega)} + \|\psi\|_{L^2(\Omega)}.$$

Proof. Owing to the assumptions (2) it suffices to prove the theorem for $\mathbb{A} = \mathbb{I}$ and $\gamma = 1$. Expanding the terms in the least-squares functional yields

$$(14) \quad \begin{aligned} 2\mathcal{J}((\phi, \mathbf{v}), (\psi, \mathbf{u}); 0) &= \|\mathbf{u}\|_0^2 + 2\|\nabla \cdot \mathbf{u}\|_0^2 + 2\|\nabla \phi\|_0^2 + \|\phi\|_0^2 + \|\mathbf{v}\|_0^2 + \|\psi\|_0^2 \\ &+ 2(\mathbf{u}, \nabla \phi) + 2(\nabla \cdot \mathbf{u}, \phi) + 2(\mathbf{v}, \nabla \phi) + 2(\nabla \cdot \mathbf{u}, \psi). \end{aligned}$$

The sum of the first two inner-products vanishes for homogeneous boundary conditions

$$2(\mathbf{u}, \nabla \phi) + 2(\nabla \cdot \mathbf{u}, \phi) = 2 \int_{\partial\Omega} \phi(\mathbf{u} \cdot \mathbf{n}) \, dS = 0.$$

For the remaining two inner products we use the Young's inequality:

$$2(\mathbf{v}, \nabla\phi) \geq -\delta\|\mathbf{v}\|_0^2 - \frac{1}{\delta}\|\nabla\phi\|_0^2 \quad \text{and} \quad 2(\nabla \cdot \mathbf{u}, \psi) \geq -\delta\|\psi\|_0^2 - \frac{1}{\delta}\|\nabla \cdot \mathbf{u}\|_0^2.$$

Combining with (14) yields

$$2\mathcal{J}((\phi, \mathbf{v}), (\psi, \mathbf{u}); 0) \geq \|\mathbf{u}\|_0^2 + \left(2 - \frac{1}{\delta}\right)(\|\nabla \cdot \mathbf{u}\|_0^2 + \|\nabla\phi\|_0^2) + \|\phi\|_0^2 + (1 - \delta)(\|\mathbf{v}\|_0^2 + \|\psi\|_0^2)$$

The theorem follows by choosing any $1/2 < \delta < 1$. \square

The next result provides some information about the conservation properties of (12).

Proposition 1. *The minimizers of (11) satisfy (10) in $L^2(\Omega)$.*

Proof. The variations of the least-squares functional in (11) with respect to \mathbf{v} and ψ yield the equations

$$(15) \quad \int_{\Omega} (\mathbf{v} + \nabla\phi) \cdot \tilde{\mathbf{v}} \, dx = 0 \quad \forall \tilde{\mathbf{v}} \in L^2(\Omega) \quad \text{and} \quad \int_{\Omega} (\nabla \cdot \mathbf{u} + \psi - f)\tilde{\psi} \, dx = 0 \quad \forall \tilde{\psi} \in L^2(\Omega),$$

respectively. The minimizers of (11) necessarily satisfy these equations, which implies that (10) hold in L^2 -sense. \square

Proposition 2. *If (10) is satisfied in $L^2(\Omega)$, then the equations for ϕ and \mathbf{u} decouple.*

Proof. The variations of the least-squares functional in (11) with respect to \mathbf{u} and ϕ yield the equations

$$\int_{\Omega} \gamma^{-1} \nabla \cdot \mathbf{u} \nabla \cdot \tilde{\mathbf{u}} \, dx + \int_{\Omega} \mathbf{u} \mathbb{A}^{-1} \tilde{\mathbf{u}} \, dx - \int_{\Omega} \gamma^{-1} f \nabla \cdot \tilde{\mathbf{u}} \, dx = \int_{\Omega} (\nabla \cdot \mathbf{u} + \psi - f) \nabla \cdot \tilde{\mathbf{u}} \, dx,$$

and

$$\int_{\Omega} \nabla\phi \mathbb{A} \nabla\tilde{\phi} \, dx + \int_{\Omega} \gamma\phi\tilde{\phi} \, dx - \int_{\Omega} f\tilde{\phi} = \int_{\Omega} (\mathbf{v} + \nabla\phi) \nabla\tilde{\phi} \, dx,$$

for all $\tilde{\mathbf{u}} \in H(\text{div}, \Omega)$ and $\tilde{\phi} \in H^1(\Omega)$, respectively. Proposition 1 shows that the right hand side of these variational statements vanishes and therefore the equations for ϕ and \mathbf{u} decouple. See also [3] for a similar decoupling in a constrained formulation. \square

2.1. A mimetic least-squares method. Suppose that $U^h = G^h \times C^h$ and $V^h = S^h \times D^h$ are compatible finite element discretizations of U and V such that $\{G^h, C^h\}$ and $\{D^h, S^h\}$ belong in a discrete DeRham complex [1, 11]. In other words, there holds

$$(16) \quad \nabla\phi^h \in C^h \quad \forall \phi^h \in G^h \quad \text{and} \quad \nabla \cdot \mathbf{u}^h \in S^h \quad \forall \mathbf{u}^h \in D^h.$$

We define the mimetic least-squares principle for (9) as the restriction of (12) to the discrete spaces U^h and V^h :

$$(17) \quad \min_{(\phi^h, \mathbf{v}^h) \in U^h, (\psi^h, \mathbf{u}^h) \in V^h} \mathcal{J}((\phi^h, \mathbf{v}^h), (\psi^h, \mathbf{u}^h); f).$$

Because U^h and V^h are conforming spaces, the norm equivalence (13) continues to hold and (17) is a well-posed minimization problem. In addition, the least-squares solution is *locally conservative*.

Theorem 2. *Let $\{(\phi^h, \mathbf{v}^h), (\psi^h, \mathbf{u}^h)\} \in U^h \times V^h$ be a minimizer of (17). Then,*

$$(18) \quad \mathbf{v}^h + \nabla\phi^h = 0 \quad \text{and} \quad \nabla \cdot \mathbf{u}^h + \psi^h = P_S f$$

where P_S is the L^2 projection on S^h .

Proof. Consider first the gradient equation in (18). The minimizers of (17) necessarily satisfy the equations

$$\int_{\Omega} (\mathbf{v}^h + \nabla \phi^h) \cdot \tilde{\mathbf{v}}^h \, dx = 0 \quad \forall \tilde{\mathbf{v}}^h \in C^h$$

Since $\nabla \phi^h \in C^h$ there exists $\mathbf{v}_{\phi}^h = -\nabla \phi^h$ and so, the first equation holds for the pair $\{\phi^h, \mathbf{v}_{\phi}^h\}$. By the uniqueness of the least-squares minimizer it follows that $\mathbf{v}^h = \mathbf{v}_{\phi}^h$.

Consider now the second equation in (18). The weak equation

$$\int_{\Omega} (\nabla \cdot \mathbf{u}^h + \psi^h - f) \tilde{\psi}^h \, dx \equiv \int_{\Omega} (\nabla \cdot \mathbf{u}^h + \psi^h - P_S f) \tilde{\psi}^h \, dx = 0 \quad \forall \tilde{\psi}^h \in S^h,$$

is a necessary condition for (17). Since $\nabla \cdot \mathbf{u}^h \in S^h$ there exists ψ_u^h such that $\nabla \cdot \mathbf{u}^h + \psi_u^h = P_S f$. Again, the uniqueness of the least-squares solution implies that $\psi^h = \psi_u^h$. \square

Corollary 1. *Let $\{(\phi^h, \mathbf{v}^h), (\psi^h, \mathbf{u}^h)\} \in U^h \times V^h$ then the discrete equations for ϕ^h and \mathbf{u}^h decouple in the variational formulation.*

Proof. Take variations with respect to ϕ^h and \mathbf{u}^h to obtain weak forms similar to the ones in the proof Proposition 2 and use the fact that $U^h \times V^h$ is a conforming subspace of $(H^1(\Omega), L^2(\Omega)) \times (L^2(\Omega), H(\text{div}, \Omega))$ which implies that Theorem 2 also holds on the finite dimensional subspace. \square

Remark 1. *Note that the results of Theorem 2 and Corollary 1 do not require U^h and V^h to be defined on the same grid. Thus, in principle, one can implement the least-squares method (17) using two different grid partitions of these spaces, i.e., we can consider formulations in which the gradient and divergence equations live on different grids.*

The possibility to satisfy (10) in a discrete setting brings up an intriguing question. Suppose that instead of augmenting a standard least-squares functional to obtain (11) we start directly with a least-squares principle for (9)

$$(19) \quad \min_{(\phi, \mathbf{v}), (\psi, \mathbf{u})} \mathcal{J}((\phi, \mathbf{v}), (\psi, \mathbf{u}); f) := \frac{1}{2} \left(\|\mathbb{A}^{-1/2}(\mathbf{u} - \mathbb{A}\mathbf{v})\|_0^2 + \|\gamma^{-1/2}(\gamma\phi - \psi)\|_0^2 + \|\mathbf{v} + \nabla\phi\|_0^2 + \|\nabla \cdot \mathbf{u} + \psi - f\|_0^2 \right).$$

and then proceed to discretize it using the exact same spaces U^h and V^h as in (17). Will then the solution of (19) also satisfy exactly the conservation laws (10)? Theoretical studies [4] suggest that this may not be the case, even though the discrete spaces can support the exact representation of the conservation laws. In Section 7 we present numerical results that confirm these conclusions.

To understand the root cause for the different properties of (11) and (19) note that variations of (19) with respect to \mathbf{v} and ψ yield the equations

$$\int_{\Omega} (\mathbf{v} + \nabla\phi) \cdot \tilde{\mathbf{v}} \, dx = \int_{\Omega} (\mathbb{A}\mathbf{v} - \mathbf{u}) \cdot \tilde{\mathbf{v}} \, dx \quad \forall \tilde{\mathbf{v}} \quad \text{and} \quad \int_{\Omega} (\nabla \cdot \mathbf{u} + \psi - f) \tilde{\psi} \, dx = \int_{\Omega} (\psi - \gamma\phi) \tilde{\psi} \, dx \quad \forall \tilde{\psi}$$

These equations imply that (10) hold with an error *proportional to the error in the constitutive laws*. As we shall see in Section 5, the latter cannot be satisfied exactly in a discrete setting, except in a few special cases beyond the scope of this paper. As a result, it follows that solutions of (19) may not satisfy (10) exactly even if the discrete spaces allow it.

3. TOPOLOGICAL DISCRETIZATIONS OF THE DIFFERENTIAL EQUATIONS

In this paper we focus on developing a fully conservative *spectral* least-squares formulation based on (17). In order to preserve the topological nature of the conservation laws in (10) we choose to work with spectral elements having geometrically localized degrees of freedom. These degrees of freedom live on k -dimensional mesh entities, i.e., they are k -cochains [8]. This reduces the action of gradient, curl and divergence on spectral element fields to the action of the coboundary operator on 0, 1 and 2-cochains. As a result, the discrete differential operators assume particularly simple algebraic forms and can be evaluated by *operating directly on the degrees of freedom* without reference to the basis functions. The next section reviews the relevant notions from algebraic topology.

3.1. Basic concepts from algebraic topology. For the purposes of this paper it suffices to consider the quadrilateral shown in Fig. 1. A k -chain is a formal linear combination of k -dimensional entities. Our quadrilateral incorporates three different chains: the 0-chain $c_0 = A + B + C + D$ (the vertices), the 1-chain $c_1 = C_1 + C_2 - C_3 - C_4$ (the edges, or sides) and the 2-chain $c_2 = S$, which is the quadrilateral itself. The boundary of a k -chain is a $k - 1$ -dimensional chain. For instance,

$$\begin{aligned} \partial S &= C_1 + C_2 - C_3 - C_4, \\ \partial C_1 &= -A + B \quad \partial C_2 = -B + C \quad \partial C_3 = C - D \quad \text{and} \quad \partial C_4 = -A + D. \end{aligned}$$

The $k - 1$ chains resulting from the application of ∂ reflect the orientations of the entities involved. Note that

$$(20) \quad \partial \partial S = (-A + B) + (-B + C) - (C - D) - (-A + D) = 0.$$

The identity $\partial \partial = 0$ is a fundamental property of the boundary operator. The set of all

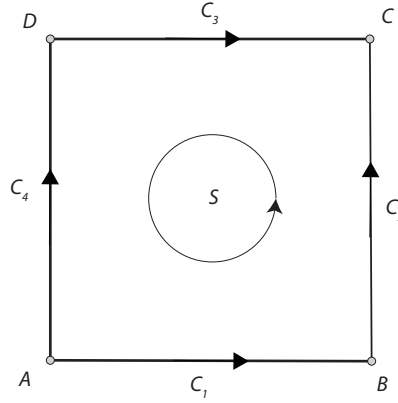


FIGURE 1. A quadrilateral is a chain complex comprising a 0-chain $\{A, B, C, D\}$ (the vertices), 1-chain $\{C_1, C_2, C_3, C_4\}$ (the edges) and a 2-chain $\{S\}$ (the cell itself). The discrete gradient relation along curve C_1 is given by (23) and involves the action of the coboundary operator δ on the 0-cochain $\{\phi_A, \phi_B\}$. This operator is dual to the boundary $\partial C_1 = B - A$, which makes it dependent only on the connectivity between the vertices and the line segments, but not on the shape of the cell.

k -chains is a linear space C_k and C^k is its dual. We associate the elements of C^k , called k -cochains, with numbers living on the k -chains of C_k . Returning to the example in Fig. 1 this means that the 0-cochain $\{\phi_A, \phi_B, \phi_C, \phi_D\}$, the 1-cochain $\{u_1, u_2, u_3, u_4\}$, and the 2-cochain $\{\psi_S\}$ correspond to values living on the vertices, edges and the quadrilateral itself. The adjoint of ∂ is called the *coboundary operator* and denoted by δ . The coboundary operator maps k -cochains into $(k + 1)$ -cochains:

$$\delta\{\phi_A, \phi_B, \phi_C, \phi_D\} = \{-\phi_A + \phi_B, -\phi_B + \phi_C, \phi_C - \phi_D, -\phi_A + \phi_D\}$$

The identity $\partial\partial = 0$ implies a similar identity $\delta\delta = 0$ for the coboundary. For example,

$$\delta\delta\{\phi_A, \phi_B, \phi_C, \phi_D\} = (-\phi_A + \phi_B) + (-\phi_B + \phi_C) - (\phi_C - \phi_D) - (-\phi_A + \phi_D) = 0 .$$

is the analogue of (20).

3.2. Mimetic approach for the differential equations. Mimetic methods use coordinate-independent representations of differential operators to derive the discrete equations; see e.g., [22] and [5]. Application of this approach to (10) leads naturally to approximation of fields and derivatives by cochains and coboundary, respectively. Let us start with the gradient equation

$$(21) \quad \mathbf{v} + \nabla\phi = 0 .$$

Mimetic discretization of (21) requires a coordinate-independent representation of the gradient. Given any curve $C \in \Omega$ with endpoints A, B integration of (21) from A to B yields

$$(22) \quad 0 = \int_C (\mathbf{v} + \nabla\phi) = \phi(B) - \phi(A) + \int_C \mathbf{v} .$$

This reduces the differential equation (21) to an algebraic equation

$$(23) \quad \mathbf{v}_C + \phi_B - \phi_A = 0 ,$$

where $\phi_A = \phi(A)$, $\phi_B = \phi(B)$ and $\mathbf{v}_C := \int_C \mathbf{v}$. Note that if ϕ and \mathbf{v} satisfy the continuum equation (21) this relation is true for all points A and B and any curve C which connects these points. Note also that (23) is independent of any *material* or *mesh parameters*.

The curve C with its two endpoints forms a chain complex comprising the 0-chain $-A + B$ and the 1-chain C . Furthermore, the values $\{\phi_A, \phi_B\}$ and $\{\mathbf{v}_C\}$ define 0 and 1-cochains associated with the endpoints and the curve, respectively. This allows us to write (23) as

$$(24) \quad \mathbf{v}_C + \delta\{\phi_A, \phi_B\} = 0 .$$

This equation is the mimetic discretization of (21) along C . In particular, the coboundary acting on 0-cochains gives the mimetic discretization of the gradient.

Extension of (24) to the (oriented) mesh cell in Figure 1 is straightforward. We approximate ϕ by the 0-cochain $\{\phi_A, \phi_B, \phi_C, \phi_D\}$ and the vector field \mathbf{v} by the 1-cochain $\{\mathbf{v}_{C_1}, \mathbf{v}_{C_2}, \mathbf{v}_{C_3}, \mathbf{v}_{C_4}\}$. As a result, (21) reduces to a set of four algebraic equations:

$$\left\{ \begin{array}{ll} \mathbf{v}_{C_1} + \delta\{\phi_A, \phi_B\} = 0 & \text{and} \quad \mathbf{v}_{C_3} + \delta\{\phi_C, \phi_D\} = 0 \\ \mathbf{v}_{C_2} + \delta\{\phi_B, \phi_C\} = 0 & \mathbf{v}_{C_4} + \delta\{\phi_D, \phi_A\} = 0 \end{array} \right. ,$$

where

$$\begin{aligned} \delta\{\phi_A, \phi_B\} &= -\phi_A + \phi_B; & \delta\{\phi_B, \phi_C\} &= \phi_C - \phi_B; & \delta\{\phi_C, \phi_D\} &= \phi_C - \phi_D; \\ \text{and} \quad \delta\{\phi_D, \phi_A\} &= \phi_D - \phi_A \end{aligned} ,$$

are the restrictions of the coboundary to the endpoints of the edges.

Since integrals are additive, we have for the closed contour (1-chain) $C = C_1 + C_2 - C_3 - C_4$ that

$$(25) \quad \mathbf{v}_{C_1} + \mathbf{v}_{C_2} - \mathbf{v}_{C_3} - \mathbf{v}_{C_4} = -\phi_B + \phi_A - \phi_C + \phi_B + \phi_C - \phi_D + \phi_D - \phi_A \equiv 0,$$

or, in terms of the coboundary,

$$(26) \quad \delta\{\mathbf{v}_{C_1}, \mathbf{v}_{C_2}, \mathbf{v}_{C_3}, \mathbf{v}_{C_4}\} = \delta\delta\{\phi_A, \phi_B, \phi_C, \phi_D\} = 0.$$

This relation is a discrete version of the identity

$$(27) \quad \mathbf{v}_C \equiv \int_C \mathbf{v} = \int_S \nabla \times \mathbf{v} \equiv 0$$

that holds on any surface S with boundary $\partial S = C$, provided \mathbf{v} is a gradient. Simply put (26) means that (i) the action of coboundary on a 1-cochain approximates the action of curl on a vector field, and (ii) the identity $\nabla \times (\nabla\phi) = 0$ also holds at the discrete level.

Note again that this discrete notion of the curl does not involve any mesh parameters; it holds on very coarse meshes and very fine mesh. There is no truncation error, no asymptotic regime, no need to consider these equations in the limit $h \rightarrow 0$. We will refer to such discretizations as *topological* and we call the discrete equations *exact*.

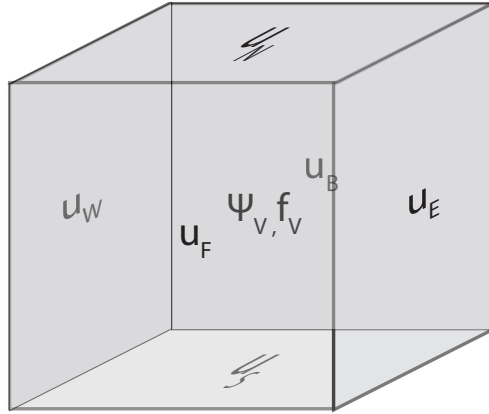


FIGURE 2. The fluxes $\mathbf{u}_W, \mathbf{u}_E, \mathbf{u}_S, \mathbf{u}_N, \mathbf{u}_F$, and \mathbf{u}_B form a 2-cochain associated with the 2-chain comprising the West, East, South, North, Front and Back sides of the volume. The volume integrals over f and ψ are 3-cochains $f_{\mathcal{V}}$ and $\psi_{\mathcal{V}}$, respectively.

Mimetic discretization of the second conservation relation,

$$(28) \quad \nabla \cdot \mathbf{u} + \psi = f,$$

requires a coordinate-free approximation of the divergence. This approximation is best explained in \mathbb{R}^3 . To this end, consider a three-dimensional volume, \mathcal{V} , see Figure 2. We can think of \mathcal{V} as a chain complex comprising a 3-chain given by \mathcal{V} itself, and the 2-chain $-\mathcal{S}_W + \mathcal{S}_E - \mathcal{S}_S + \mathcal{S}_N - \mathcal{S}_F + \mathcal{S}_B$, where the subscripts stand for West, East, South, North, Front and Back surfaces of \mathcal{V} . The minus signs reflect the orientation of $\mathcal{S}_W, \mathcal{S}_S$ and \mathcal{S}_F by a unit normal pointing into the volume. The rest of the surfaces are oriented by a unit

normal pointing outwards. As a result, integration of (28) on \mathcal{V} reduces it to an algebraic equation

$$(29) \quad \mathbf{u}_E - \mathbf{u}_W + \mathbf{u}_N - \mathbf{u}_S + \mathbf{u}_B - \mathbf{u}_F + \psi_{\mathcal{V}} = f_{\mathcal{V}} .$$

where

$$f_{\mathcal{V}} := \int_{\mathcal{V}} f; \quad \mathbf{u}_{\star} := \int_{S_{\star}} \mathbf{u} \cdot \mathbf{n}, \quad \star \in \{E, W, N, S, F, B\} \quad \text{and} \quad \psi_{\mathcal{V}} = \int_{\mathcal{V}} \psi .$$

The fluxes $\{\mathbf{u}_E, \mathbf{u}_W, \mathbf{u}_N, \mathbf{u}_S, \mathbf{u}_B, \mathbf{u}_F\}$ represent a 2-cochain associated with the surfaces of \mathcal{V} , whereas $f_{\mathcal{V}}$ and $\psi_{\mathcal{V}}$ are 3-cochains living on the volume itself. As a result, we can write (29) as

$$\delta\{\mathbf{u}_E, \mathbf{u}_W, \mathbf{u}_N, \mathbf{u}_S, \mathbf{u}_B, \mathbf{u}_F\} + \psi_{\mathcal{V}} = f_{\mathcal{V}} ,$$

that is, the action of δ on 2-cochains represents the divergence. Note again that this discrete representation holds for arbitrarily shaped volumes and that this expression does not depend on basis functions.

Remark 2. *The variables ϕ and ψ , and \mathbf{v} and \mathbf{u} are called dual variables. If one variable is associated with k -dimensional objects, its dual variable is associated to $(n-k)$ -dimensional objects, where $n = \dim(\Omega)$. If a dual grid structure is employed, [5, 6, 12, 16, 21, 20, 23], the discrete Hodge matrix, which maps variables associated with k -dimensional entities to variables associated with $(n-k)$ -dimensional entities is a square, invertible matrix. The latter is essential for finite volume and finite element methods. Least-squares methods allow for a non-square Hodge matrix thus alleviating the need for a strict primal-dual grid structure in mimetic least-squares methods. This is a direct consequence of Theorem 2 and Corollary 1. See also Remark 1.*

4. SPECTRAL BASIS FUNCTIONS

In this section we derive spectral basis functions on tensor product elements (quadrilaterals and hexahedrals) with geometrically localized degrees of freedom. In so doing we are able to obtain topological discretizations of the conservation laws (21) and (28) that depend only on the mesh topology. This in turn provides an effective means to implement the mimetic least-squares method presented in Section 2.

We need four different kinds of spectral basis functions to approximate

- a scalar function represented on the mesh by a 0-cochain, i.e., its nodal values;
- a vector field represented on the mesh by a 1-cochain, i.e., its line integrals along edge segments of the mesh;
- a vector field represented on the mesh by a 2-cochain, i.e., its surface integrals along surface segments of the mesh; and
- a scalar function represented on the mesh by a 3-cochain, i.e., its integrals over mesh subvolumes.

Accordingly, we refer to these as the k -cochain spectral basis functions. Let \mathcal{R}^k be the operator that reduces a particular field to a k -cochain $\{a_1^k, \dots, a_n^k\}$. Following [5] we want to define a basis $\{s_i^k\}$ such that the corresponding reconstruction operator

$$\mathcal{I}^k := \sum_{i=1}^n a_i^k s_i^k$$

has the following properties:

- $\mathcal{R}^k \circ \mathcal{I}^k = \mathbb{I}$, \mathcal{I}^k is a right-inverse of \mathcal{R}^k , (consistency property);

- $\mathcal{I}^k \circ \mathcal{R}^k = \mathbb{I} + \mathcal{O}(h^p)$, \mathcal{I}^k is an approximate left-inverse of \mathcal{R}^k , (approximation property)
- $d^k \mathcal{I}^k = \mathcal{I}^{k+1} \delta$, where d^k represents the gradient ($k = 0$), curl ($k = 1$) or divergence ($k = 2$), respectively, and δ the coboundary operator.

We define the k -cochain spectral basis functions by tensor products of one-dimensional basis functions. For brevity, we present the details in two-dimensions. In this case, construction of the spectral bases relies on two different types of one-dimensional basis functions. We review these next.

4.1. One-dimensional spectral basis functions. Consider the partitioning of the one-dimensional domain $-1 = \xi_0 < \xi_1 < \dots < \xi_{N-1} < \xi_N = 1$ comprising $N + 1$ nodes, ξ_i and N intervals (edges) $[\xi_{i-1}, \xi_i]$. We define two families of basis functions associated with the nodes and the edges of the partition, respectively.

4.1.1. *Nodal basis functions.* Let $f(\xi)$, $\xi \in [-1, 1]$ be smooth function. The reduction of $f(\xi)$ to a 0-cochain on the mesh is given by

$$(30) \quad \mathcal{R}^0(f) = \{f_0, f_1, \dots, f_N\},$$

where $f_i := f(\xi_i)$ are its nodal values. Consider the Lagrange polynomials $\ell_i^0(\xi)$ given by

$$\ell_i^0(\xi) = \prod_{\substack{j=0 \\ j \neq i}}^N \left(\frac{\xi - \xi_j}{\xi_i - \xi_j} \right).$$

We recall that Lagrange polynomials satisfy

$$\ell_i^0(\xi_j) = \begin{cases} 1 & \text{if } i = j \\ 0 & \text{if } i \neq j \end{cases} \quad \text{and} \quad \sum_{i=0}^N \ell_i^0(\xi) \equiv 1.$$

The corresponding reconstruction of $f(\xi)$ from the 0-cochain $\mathcal{R}^0(f)$ is given by

$$\mathcal{I}^0(f_i)(\xi) = \sum_{i=0}^N f_i \ell_i^0(\xi).$$

Reduction of this reconstruction gives the same discrete values

$$\mathcal{R}^0(\mathcal{I}^0(f_i)(\xi)) = \sum_{j=0}^N f_j \ell_j^0(\xi_i) = f_i,$$

and so, \mathcal{I}^0 satisfies the consistency property, $\mathcal{R}^0 \circ \mathcal{I}^0 = \mathbb{I}$. For suitably chosen nodes ξ_i and sufficiently smooth $f(\xi)$ one can show that $\mathcal{I}^0 \circ \mathcal{R}^0 = \mathbb{I} + \mathcal{O}(h^p)$. Figure 3 illustrates this property.

4.1.2. *Edge basis functions.* We consider again a smooth function $f(\xi)$ but reduce it to a 1-cochain given by

$$(31) \quad \mathcal{R}^1(f) = \{f_1, \dots, f_N\},$$

where now the degrees of freedom

$$f_i = \int_{\xi_{i-1}}^{\xi_i} f(\xi), \quad i = 1, \dots, N.$$

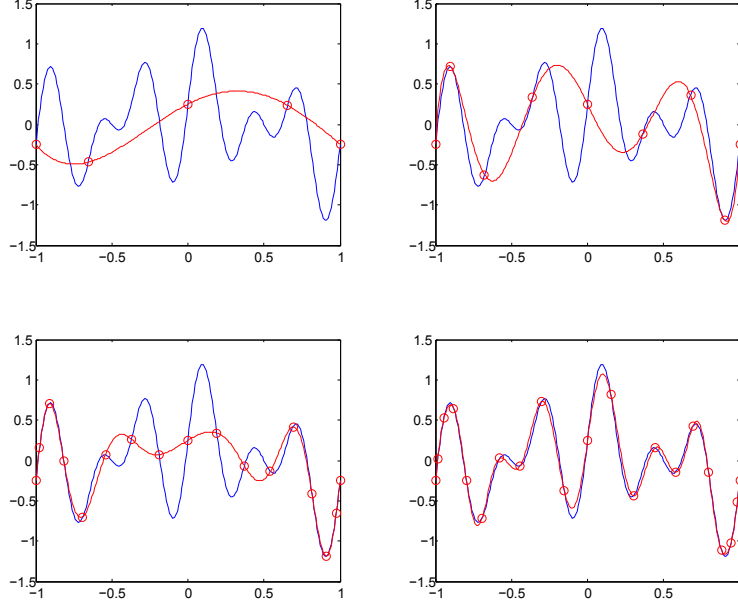


FIGURE 3. Nodal approximation (red curve) of $f(\xi) = \cos \pi\xi(\sin 5\pi\xi + 0.25)$, (blue curve) for $N = 4, 8, 16, 20$.

are the *edge* integrals of f . Define the edge Lagrangian basis, $\ell_i^1(\xi)$ by [13, 21]

$$(32) \quad \ell_i^1(\xi) = -\frac{d}{d\xi} \sum_{k=0}^{i-1} \ell_k^0(\xi), \quad i = 1, \dots, N.$$

From this definition of edge basis functions it follows that

$$(33) \quad \ell_0^1(\xi) = 0 \quad \text{and} \quad \ell_{N+1}^1(\xi) = -\frac{d}{d\xi} \sum_{k=0}^N \ell_k^0(\xi) = -\frac{d}{d\xi}(1) = 0.$$

The edge basis functions have the property that

$$(34) \quad \int_{\xi_{j-1}}^{\xi_j} \ell_i^1 = \begin{cases} 1 & \text{if } i = j \\ 0 & \text{if } i \neq j \end{cases}, \quad i, j = 1, \dots, N.$$

The reconstruction of $f(\xi)$ from the 1-cochain $\mathcal{R}^1(f)$ is given by

$$(35) \quad \mathcal{I}^1(f_i)(\xi) = \sum_{i=1}^N f_i \ell_i^1(\xi).$$

The reduction of the reconstructed function gives

$$(36) \quad \mathcal{R}^1(\mathcal{I}^1(f_i)(\xi)) = \sum_{i=1}^N f_i \int_{\xi_{j-1}}^{\xi_j} \ell_i^1 \stackrel{(34)}{=} f_j,$$

which shows that consistency property, $\mathcal{R}^1 \circ \mathcal{I}^1 = \mathbb{I}$, is satisfied. Figure 4 shows that for increasing N the accuracy of the reconstruction improves, $\mathcal{I}^1 \circ \mathcal{R}^1 = \mathbb{I} + \mathcal{O}(h^p)$. Figures 3–4 also clearly demonstrate the difference between \mathcal{I}^0 , which matches the *nodal values* of a

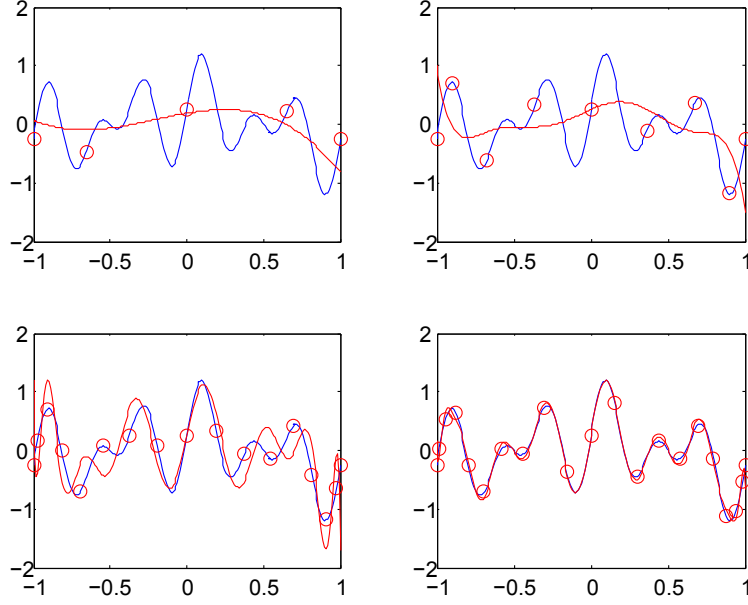


FIGURE 4. Edge basis approximation (red curve) of $f(x) = \cos \pi x (\sin 5\pi x + 0.25)$ (blue curve), for $N = 4, 8, 16, 20$.

function and \mathcal{I}^1 which matches the *edge integrals* of a function. In particular, $\mathcal{I}^1(f_i)(\xi)$ does not pass through the nodal values f_i , shown by red circles in the figure, i.e., this reconstruction is not nodal.

Finally we need to show that the nodal reconstruction \mathcal{I}^0 and the edge reconstruction \mathcal{I}^1 commute with differentiation at the continuous and discrete level. Let $f(\xi)$ be a smooth function with reduction given by (30):

$$\mathcal{R}^0(f) = \{f_0, \dots, f_N\}.$$

The coboundary, δ applied to this 0-cochain gives

$$\delta \mathcal{R}^0(f) = \{f_1 - f_0, \dots, f_N - f_{N-1}\}.$$

On the other hand, the reduction of its derivative $\frac{d}{d\xi} f(\xi)$ to a 1-cochain gives

$$(37) \quad \mathcal{R}^1\left(\frac{d}{d\xi} f\right) = \int_{\xi_{i-1}}^{\xi_i} \frac{d}{d\xi} f(\xi) d\xi = f_i - f_{i-1},$$

which shows that $\delta \mathcal{R}^0 = \mathcal{R}^1 \frac{d}{d\xi}$, see [5].

The reconstruction of the 1-cochain $\{f_1 - f_0, \dots, f_N - f_{N-1}\}$ is given by

$$(38) \quad \mathcal{I}^1(\delta f)(\xi) = \sum_{i=1}^N (f_i - f_{i-1}) \ell_i^1(\xi).$$

The reconstruction of the 0-cochain $\{f_0, \dots, f_N\}$ is given by

$$\mathcal{I}^0(f)(\xi) = \sum_{i=0}^N f_i \ell_i^0(\xi).$$

Differentiation of this reconstruction yields

$$\begin{aligned} \frac{d}{d\xi} \mathcal{I}^0(f)(\xi) &= \frac{d}{d\xi} \sum_{i=0}^N f_i \ell_i^0(\xi) = \sum_{i=0}^N f_i \frac{d}{d\xi} \ell_i^0(\xi) \\ &\stackrel{(32)}{=} -f_0 \ell_1^1(\xi) + \sum_{i=1}^{N-1} f_i [\ell_i^1(\xi) - \ell_{i+1}^1(\xi)] + f_N \ell_N^1(\xi) \\ &\stackrel{(33)}{=} \sum_{i=0}^N f_i [\ell_i^1(\xi) - \ell_{i+1}^1(\xi)] \\ (39) \quad &= \sum_{i=1}^N (f_i - f_{i-1}) \ell_i^1(\xi). \end{aligned}$$

From (38) and (39) we see that the commuting property $\frac{d}{d\xi} \mathcal{I}^0 = \mathcal{I}^1 \delta$ holds.

4.2. Two-dimensional 0-cochain and 1-cochain spectral basis functions. Topological discretization of the gradient equation $\mathbf{v} + \nabla \phi = 0$ requires approximation of ϕ and \mathbf{v} by 0-cochains and 1-cochains, respectively. We use a tensor product structure to define the corresponding spectral basis functions from the one-dimensional nodal and edge basis functions as follows. Consider the unit square $[-1, 1]^2 \subset \mathbb{R}^2$ with partitioning $-1 = \xi_0 < \dots < \xi_N = 1$ and $-1 = \eta_0 < \dots < \eta_M = 1$. On this mesh we have two sets of nodal basis functions given by the Lagrange polynomials

$$\ell_i^0(\xi), \quad i = 0, \dots, N \quad \text{and} \quad \ell_j^0(\eta), \quad j = 0, \dots, M,$$

respectively, and two sets of edge basis functions given by

$$\ell_i^1(\xi), \quad i = 1, \dots, N \quad \text{and} \quad \ell_j^1(\eta), \quad j = 1, \dots, M,$$

respectively.

The reduction of a smooth function $\phi(\xi, \eta)$ to a 0-cochain is given by

$$\mathcal{R}^0(\phi) = \{\phi_{i,j}\}_{i=0,j=0}^{N,M},$$

where $\phi_{i,j} := \phi(\xi_i, \eta_j)$, i.e., it consists of sampling its values at the points (ξ_i, η_j) . The corresponding reconstruction is then given by

$$(40) \quad \mathcal{I}^0(\phi_{i,j})(\xi, \eta) = \sum_{i=0}^N \sum_{j=0}^M \phi_{i,j} \ell_i^0(\xi) \ell_j^0(\eta),$$

and its gradient by

$$(41) \quad \nabla \mathcal{I}^0(\phi_{i,j})(\xi, \eta) = \sum_{i=1}^N \sum_{j=0}^M (\phi_{i,j} - \phi_{i-1,j}) \ell_i^1(\xi) \ell_j^0(\eta) + \sum_{i=0}^N \sum_{j=1}^M (\phi_{i,j} - \phi_{i,j-1}) \ell_i^0(\xi) \ell_j^1(\eta).$$

The reduction of a smooth vector field $\mathbf{v} = (u, v)$ to a 1-cochain on this grid is given by

$$\mathcal{R}^1(\mathbf{v}) := \{u_{i,j}, v_{l,l}\}_{i=1,j=0,k=0,l=1}^{N,M,N,M},$$

where

$$(42) \quad u_{i,j} = \int_{\xi_{i-1}}^{\xi_i} u|_{\eta=\eta_j} = \int_{\xi_{i-1}}^{\xi_i} u(\xi, \eta_j) d\xi, \quad i = 1, \dots, N \text{ and } j = 0, \dots, M,$$

and

$$(43) \quad v_{i,j} = \int_{\eta_{j-1}}^{\eta_j} v|_{\xi=\xi_i} = \int_{\eta_{j-1}}^{\eta_j} v(\xi_i, \eta) d\eta, \quad i = 0, \dots, N \text{ and } j = 1, \dots, M.$$

In words, we represent this vector field by using integrals of its *tangential component* on the horizontal and vertical subedges of the element. The corresponding reconstruction is then given by

$$(44) \quad \mathcal{I}^1(\mathbf{v}_{i,j})(\xi, \eta) = \sum_{i=1}^N \sum_{j=0}^M u_{i,j} \ell_i^1(\xi) \ell_j^0(\eta) + \sum_{i=0}^N \sum_{j=1}^M v_{i,j} \ell_i^0(\xi) \ell_j^1(\eta).$$

The discrete analogue of the gradient relation $\mathbf{v} + \nabla\phi = 0$ expressed in terms of the expansions (41) and (44) then gives

$$\begin{aligned} \mathcal{I}^1(\mathbf{v}_{i,j}) + \nabla \mathcal{I}^0(\phi_{i,j}) &= \sum_{i=1}^N \sum_{j=0}^N u_{i,j} \ell_i^1(\xi) \ell_j^0(\eta) + \sum_{i=0}^N \sum_{j=1}^N v_{i,j} \ell_i^0(\xi) \ell_j^1(\eta) \\ &+ \sum_{i=1}^N \sum_{j=0}^N (\phi_{i,j} - \phi_{i-1,j}) \ell_i^1(\xi) \ell_j^0(\eta) + \sum_{i=0}^N \sum_{j=1}^N (\phi_{i,j} - \phi_{i,j-1}) \ell_i^0(\xi) \ell_j^1(\eta) \\ &= \sum_{i=1}^N \sum_{j=0}^N (u_{i,j} + \phi_{i,j} - \phi_{i-1,j}) \ell_i^1(\xi) \ell_j^0(\eta) + \sum_{i=0}^N \sum_{j=1}^N (v_{i,j} + \phi_{i,j} - \phi_{i,j-1}) \ell_i^0(\xi) \ell_j^1(\eta) = 0. \end{aligned}$$

Since the bases $\ell_i^1(\xi) \ell_j^0(\eta)$ and $\ell_i^0(\xi) \ell_j^1(\eta)$ are linearly independent, the above identity holds if and only if all coefficients vanish, i.e.,

$$(45) \quad u_{i,j} + \phi_{i,j} - \phi_{i-1,j} = 0 \quad \text{and} \quad v_{i,j} + \phi_{i,j} - \phi_{i,j-1} = 0.$$

This reduces the discretization of $\mathbf{v} + \nabla\phi = 0$ to a purely algebraic relation between the degrees of freedom that does not involve the basis functions themselves. Note that equations (45) have the exact same structure as the equations we derived in (23).

4.3. Two-dimensional 2-cochain and 3-cochain spectral basis functions. These basis functions are required for the topological discretization of the divergence equation $\nabla \cdot \mathbf{u} + \psi = f$. In the three-dimensional case the flux is given by $\mathbf{u} = (p, q, r)$, where the coefficients p , q and r are functions of (ξ, η, ζ) . In the two-dimensional case, we assume that $r = 0$ and $p(\xi, \eta)$ and $q(\xi, \eta)$ only. The surface over which flux is evaluated is spanned by a line segment in (ξ, η) -space and a unit distance in the ζ -direction.

In light of Remark 1 the grid for the discretization of this equation does not have to be the same as for the gradient equation. To highlight this fact we consider a second two-dimensional grid with partitioning $-1 = \tilde{\xi}_0 < \dots < \tilde{\xi}_{\tilde{N}} = 1$ and $-1 = \tilde{\eta}_0 < \dots < \tilde{\eta}_{\tilde{M}} = 1$. To construct the spectral basis functions we will use again the one-dimensional nodal and edge bases. However, to distinguish them from the ones used in Section 4.2 we write

$$\tilde{\ell}_i^0(\xi), \quad i = 0, \dots, \tilde{N} \quad \text{and} \quad \tilde{\ell}_j^0(\eta), \quad j = 0, \dots, \tilde{M},$$

for the nodal functions, and

$$\tilde{\ell}_i^1(\xi), \quad i = 1, \dots, \tilde{N} \quad \text{and} \quad \tilde{\ell}_j^1(\eta), \quad j = 1, \dots, \tilde{M},$$

for the edge functions.

Let $\mathbf{u} = (p, q, 0)$ be a smooth vector field. In two-dimensions, reduction of this field to a 2-cochain corresponds to a representation of \mathbf{u} by using integrals of its *normal component* on the horizontal and vertical subfaces of the element. As a result, we have that

$$\mathcal{R}^2(\mathbf{u}) := \{\tilde{p}_{i,j}, \tilde{q}_{k,l}\}_{i=0,j=1,k=1,l=0}^{\tilde{N},\tilde{M},\tilde{N},\tilde{M}},$$

where

$$(46) \quad \tilde{p}_{ij} = \int_0^1 \int_{\tilde{\eta}_{j-1}}^{\tilde{\eta}_j} p|_{\xi=\tilde{\xi}_i} d\eta d\zeta = \int_{\tilde{\eta}_{j-1}}^{\tilde{\eta}_j} p(\tilde{\xi}_i, \eta) d\eta, \quad i = 0, \dots, \tilde{N} \text{ and } j = 1, \dots, \tilde{M},$$

and

$$(47) \quad \tilde{q}_{ij} = \int_0^1 \int_{\tilde{\xi}_{i-1}}^{\tilde{\xi}_i} q|_{\eta=\tilde{\eta}_j} d\xi d\zeta = \int_{\tilde{\xi}_{i-1}}^{\tilde{\xi}_i} q(\xi, \tilde{\eta}_j) d\xi, \quad i = 1, \dots, \tilde{N} \text{ and } j = 0, \dots, \tilde{M}.$$

The reconstruction of this field is then given by

$$(48) \quad \mathcal{I}^2(\mathbf{u}_{i,j})(\xi, \eta) = \sum_{i=0}^{\tilde{N}} \sum_{j=1}^{\tilde{M}} p_{i,j} \tilde{\ell}_i^0(\xi) \tilde{\ell}_j^1(\eta) - \sum_{i=1}^{\tilde{N}} \sum_{j=0}^{\tilde{M}} q_{i,j} \tilde{\ell}_i^1(\xi) \tilde{\ell}_j^0(\eta).$$

It is easy to see using (39) that

$$(49) \quad \nabla \cdot \mathcal{I}^2(\mathbf{u}_{i,j})(\xi, \eta) = \sum_{i=1}^{\tilde{N}} \sum_{j=1}^{\tilde{M}} (p_{i,j} - p_{i-1,j} + q_{i,j} - q_{i,j-1}) \tilde{\ell}_i^1(\xi) \tilde{\ell}_j^1(\eta).$$

Formally, a 3-cochain is not defined in two-dimensions. To properly formulate the reduction of a smooth scalar function required for the topological discretization of the divergence equation we extend the two-dimensional element into a box of unit height but do not subdivide the ζ -axis into subintervals as we did for the 2-cochain. Extrusion of the two-dimensional mesh along the ζ -axis partitions the box into sub-boxes forming a 3-chain. We will use this 3-chain only to obtain a proper interpretation of a 3-cochain in 2-dimensions, in practical implementation such an extrusion is not necessary.

Since ψ does not depend on ζ , using this 3-chain for the reduction yields

$$\mathcal{R}^3(\psi) = \{\tilde{\psi}_{i,j}\}_{i=1,j=1}^{\tilde{N},\tilde{M}}$$

where

$$(50) \quad \tilde{\psi}_{i,j} = \int_{\tilde{\xi}_{i-1}}^{\tilde{\xi}_i} \int_{\tilde{\eta}_{j-1}}^{\tilde{\eta}_j} \int_0^1 \psi(\xi, \eta) d\xi d\eta d\zeta = \int_{\tilde{\xi}_{i-1}}^{\tilde{\xi}_i} \int_{\tilde{\eta}_{j-1}}^{\tilde{\eta}_j} \psi(\xi, \eta) d\xi d\eta$$

The corresponding reconstruction of ψ is then given by

$$(51) \quad \mathcal{I}^3(\tilde{\psi}_{i,j})(\xi, \eta) = \sum_{i=1}^{\tilde{N}} \sum_{j=1}^{\tilde{M}} \tilde{\psi}_{i,j} \tilde{\ell}_i^1(\xi) \tilde{\ell}_j^1(\eta),$$

The topological discretization of the divergence equation also requires reduction of the data f to a 3-cochain. Using the same argument as for ψ we arrive at

$$(52) \quad \mathcal{I}^3(\tilde{f}_{i,j})(\xi, \eta) = \sum_{i=1}^{\tilde{N}} \sum_{j=1}^{\tilde{M}} \tilde{f}_{i,j} \tilde{\ell}_i^1(\xi) \tilde{\ell}_j^1(\eta),$$

with

$$(53) \quad \tilde{f}_{i,j} = \int_{\tilde{\xi}_{i-1}}^{\tilde{\xi}_i} \int_{\tilde{\eta}_{j-1}}^{\tilde{\eta}_j} f.$$

If we insert the finite dimensional approximations (49), (51) and (52) in the divergence equation $\nabla \cdot \mathbf{u} + \psi - f = 0$, we obtain

$$\begin{aligned} \nabla \cdot \mathcal{I}^2(\mathbf{u}_{i,j}) + \mathcal{I}^3(\tilde{\psi}_{i,j}) - \mathcal{I}^3(\tilde{f}_{i,j}) = \\ \sum_{i=1}^{\tilde{N}} \sum_{j=1}^{\tilde{M}} (\tilde{p}_{i,j} - \tilde{p}_{i-1,j} + \tilde{q}_{i,j} - \tilde{q}_{i,j-1} + \tilde{\psi}_{i,j} - \tilde{f}_{i,j}) \tilde{\ell}_i^1(\xi) \tilde{\ell}_j^1(\eta) = 0. \end{aligned}$$

Since the basis $\tilde{\ell}_i^1(\xi) \tilde{\ell}_j^1(\eta)$ is linearly independent, the only way in which we can satisfy this equation is for

$$(54) \quad \tilde{p}_{i,j} - \tilde{p}_{i-1,j} + \tilde{q}_{i,j} - \tilde{q}_{i,j-1} + \tilde{\psi}_{i,j} - \tilde{f}_{i,j} = 0, \quad i = 1, \dots, \tilde{N}, \quad j = 1, \dots, \tilde{M}.$$

We stress upon the fact that even though all variables are approximated by spectral elements, the discretizations of the gradient and divergence equations given by (45) and (54), respectively are purely topological. In other words, they depend only on the mesh topology but not on the size or shape of the individual elements. Compare this equation with the relation obtained in (29).

5. DISCRETIZATION OF THE CONSTITUTIVE RELATIONS

In Section 3 we developed topological discretizations of the differential equations in (9), which only involve the discrete degrees of freedom. The resulting algebraic equations are exact and depend only on the mesh topology but not on the reconstruction, i.e., on the particular choice of basis functions as long as they satisfy the reconstruction properties listed in Section 4.

Discretization of the constitutive laws

$$(55) \quad \mathbf{u} = \mathbb{A} \mathbf{v} \quad \text{and} \quad \psi = \gamma \phi.$$

presents an entirely different situation. Suppose for simplicity that $\mathbb{A} = \mathbb{I}$, $\gamma = 1$ and as before, ϕ , \mathbf{v} , \mathbf{u} , and ψ are approximated by 0,1,2 and 3-cochains, respectively. Then, in order for (55) to hold exactly we must have

$$(56) \quad \mathcal{I}^2(\mathbf{u}) = \mathcal{I}^1(\mathbf{v}) \quad \text{and} \quad \mathcal{I}^3(\psi) = \mathcal{I}^0(\phi).$$

However, it is easy to see that relationships such as (56) may not even hold true if the *same* function is reduced to different cochains and then reconstructed back, because reconstruction is only an approximate left inverse of the reduction. As a result, in general

$$\mathcal{I}^k \circ \mathcal{R}^k(f) \neq \mathcal{I}^{(n-k)} \circ \mathcal{R}^{(n-k)}(f).$$

Approximation of the smooth function $f(x) = \cos \pi \xi (\sin 5\pi \xi + 0.25)$ by node and edge basis functions in Sections 4.1.1–4.1.2 provides a simple illustration of this fact. The reconstruction from 0-cochains $\mathcal{I}^0 \circ \mathcal{R}^0(f)$ is the Lagrange nodal interpolant of $f(x)$, i.e., a polynomial that has the same nodal values on the mesh as $f(x)$. On the other hand, the reconstruction of the same function from 1-cochains, $\mathcal{I}^1 \circ \mathcal{R}^1(f)$, matches the integral of $f(x)$ on every element but not its nodal values, i.e., $\mathcal{I}^1 \circ \mathcal{R}^1(f) \neq \mathcal{I}^0 \circ \mathcal{R}^0(f)$. Figures 3 and 4 clearly show this distinction.

On the other hand, the material parameters in the constitutive laws are often determined through field observations, which introduce experimental errors. As a result, satisfying (55) exactly is not always of the same paramount importance as the exactness of the differential equations, which express fundamental physical laws. Or as Perot puts it: "*Constitutive equations are physical approximations hypothesized by humans to represent certain*

macroscopic material states. It is therefore consistent to place all the numerical approximation in the same place as the physical approximation.”, [24]. The approach outlined in Section 2 satisfies the conservation laws exactly, whereas (55) are imposed in a weak, least-squares sense. Therefore, it is consistent with the relative importance of the two groups of equations.

6. TRANSFORMATION OF DISCRETE APPROXIMATIONS

The finite dimensional representation in terms of tensor products is particularly well suited for orthogonal grids on a unit square, but in more general geometries this can be quite restrictive. In this section we will see how the various variables and equations behave under mappings.

Suppose we represent the k -cochains on the unit square with an orthogonal Gauss-Lobatto grid referred to as Ω_0 with coordinates (ξ, η) as described in Sections 4.2 and 4.3. Consider the map $\Phi : \Omega_0 \rightarrow \Omega$ with coordinates $(x, y) = \Phi(\xi, \eta)$. This transformation will map the point $(\xi_i, \eta_j) \in \Omega_0$ onto $\Phi(\xi_i, \eta_j) \in \Omega$ and the line segment $(\xi, \eta_j) \in \Omega_0$, for $\xi \in [\xi_{i-1}, \xi_i]$ onto $\Phi(\xi, \eta_j) \in \Omega$ and so on.

Since we employ geometrically localized degrees of freedom corresponding to integral values, the geometric transformation Φ of the domain induces a transformation Φ^* on the cochains defined in Ω to transformed cochains defined in Ω_0 , which corresponds to a change of variables for integration. In the 2-dimensional case we can write $x = \Phi^x(\xi, \eta)$ and $y = \Phi^y(\xi, \eta)$. For the 0-cochains $\phi_{i,j}$ in Ω this means that

$$(57) \quad \phi_{i,j} := \phi(x_i, y_j) = \phi(\Phi^x(\xi_i, \eta_j), \Phi^y(\xi_i, \eta_j)) ,$$

where we consider the expression on the right hand side as a function of (ξ, η) . For the 1-cochains consider the curve $C = \Phi(C_0)$ in Ω with C_0 a curve in Ω_0 , then the 1-cochain *along* this curve is

$$\begin{aligned} v_C &= \int_C u(x, y) dx + v(x, y) dy = \int_{\Phi(C_0)} u(x, y) dx + v(x, y) dy \\ &= \int_{C_0} u(\Phi^x(\xi, \eta), \Phi^y(\xi, \eta)) \left(\frac{\partial \Phi^x}{\partial \xi} d\xi + \frac{\partial \Phi^x}{\partial \eta} d\eta \right) + v(\Phi^x(\xi, \eta), \Phi^y(\xi, \eta)) \left(\frac{\partial \Phi^y}{\partial \xi} d\xi + \frac{\partial \Phi^y}{\partial \eta} d\eta \right) \\ &= \int_{C_0} \left(u \frac{\partial \Phi^x}{\partial \xi} + v \frac{\partial \Phi^y}{\partial \xi} \right) d\xi + \left(u \frac{\partial \Phi^x}{\partial \eta} + v \frac{\partial \Phi^y}{\partial \eta} \right) d\eta , \end{aligned}$$

where we suppressed in the last line the dependence of the components u and v on ξ and η . This holds for all curves, so locally we have

$$u(x, y) dx + v(x, y) dy = \left(u \frac{\partial \Phi^x}{\partial \xi} + v \frac{\partial \Phi^y}{\partial \xi} \right) d\xi + \left(u \frac{\partial \Phi^x}{\partial \eta} + v \frac{\partial \Phi^y}{\partial \eta} \right) d\eta .$$

This equation allows us to evaluate the expression $u dx + v dy$ in (ξ, η) -coordinates. What we in fact want, is to have the expression in (ξ, η) -coordinates and bring it over to (x, y) -coordinates, because it is in these coordinates that we want to satisfy the conservation laws and the constitutive relations. Inverting this local relation gives

$$(58) \quad u d\xi + v d\eta = \frac{1}{J} \left[\left(u \frac{\partial \Phi^y}{\partial \eta} - v \frac{\partial \Phi^y}{\partial \xi} \right) dx + \left(-u \frac{\partial \Phi^x}{\partial \eta} + v \frac{\partial \Phi^x}{\partial \xi} \right) dy \right] ,$$

where $J = \frac{\partial \Phi^x}{\partial \xi} \frac{\partial \Phi^y}{\partial \eta} - \frac{\partial \Phi^x}{\partial \eta} \frac{\partial \Phi^y}{\partial \xi}$. This inverse map allows us to evaluate the cochains on the orthogonal grid and maps the result onto the curved coordinates (x, y) .

For the fluxes *over* a curve C , i.e. the 2-cochains form Section 4.3, we have that

$$\begin{aligned} \mathbf{u}_C &= \int_C p(x, y) dy - q(x, y) dx = \int_{\Phi(C_0)} p(x, y) dy - q(x, y) dx \\ &= \int_{C_0} p \left(\frac{\partial \Phi^y}{\partial \xi} d\xi + \frac{\partial \Phi^y}{\partial \eta} d\eta \right) - q \left(\frac{\partial \Phi^x}{\partial \xi} d\xi + \frac{\partial \Phi^x}{\partial \eta} d\eta \right) \\ &= \int_{C_0} \left(p \frac{\partial \Phi^y}{\partial \xi} - q \frac{\partial \Phi^x}{\partial \xi} \right) d\xi + \left(p \frac{\partial \Phi^y}{\partial \eta} - q \frac{\partial \Phi^x}{\partial \eta} \right) d\eta . \end{aligned}$$

Locally this means that

$$p dy - q dx = \left(p \frac{\partial \Phi^y}{\partial \xi} - q \frac{\partial \Phi^x}{\partial \xi} \right) d\xi + \left(p \frac{\partial \Phi^y}{\partial \eta} - q \frac{\partial \Phi^x}{\partial \eta} \right) d\eta .$$

This transformation takes takes the fluxes from (x, y) -coordinates to (ξ, η) -coordinates. The inverse relation brings the fluxes defined in (ξ, η) -coordinates over to (x, y) -coordinates.

$$(59) \quad p d\eta - q d\xi = \frac{1}{J} \left[\left(p \frac{\partial \Phi^x}{\partial \xi} + q \frac{\partial \Phi^x}{\partial \eta} \right) dy - \left(p \frac{\partial \Phi^y}{\partial \xi} + q \frac{\partial \Phi^y}{\partial \eta} \right) dx \right] .$$

We see that the fluxes *through a line* transform differently from velocities *along a line*. This is another argument to use both \mathbf{v} and \mathbf{u} as separate variable in calculations.

Finally for the 3-cochain ψ we have the local relation

$$\psi dx dy = \psi J d\xi d\eta ,$$

with inverse relation

$$(60) \quad \psi d\xi d\eta = \frac{1}{J} \psi dx dy .$$

We see that the nodal transformation of the 0-cochain ϕ , (57), transforms differently from 3-cochain, ψ , (60). Both variables are referred to as *scalar variables*, but the distinction between scalars defined in a point and scalars per volume (densities) should be taken into account in numerical calculations.

The gradient relation $\mathbf{v} + \nabla \phi = 0$ is integrated along a curve as $u d\xi + v d\eta + \frac{\partial \phi}{\partial \xi} d\xi + \frac{\partial \phi}{\partial \eta} d\eta = 0$. Transforming to (x, y) -coordinates using (58) gives

$$(61) \quad \frac{1}{J} \left[\left(\left\{ u + \frac{\partial \phi}{\partial \xi} \right\} \frac{\partial \Phi^y}{\partial \eta} - \left\{ v + \frac{\partial \phi}{\partial \eta} \right\} \frac{\partial \Phi^y}{\partial \xi} \right) dx + \left(\left\{ u + \frac{\partial \phi}{\partial \xi} \right\} \frac{\partial \Phi^x}{\partial \eta} + \left\{ v + \frac{\partial \phi}{\partial \eta} \right\} \frac{\partial \Phi^x}{\partial \xi} \right) dy \right] = 0 .$$

We see from this equation that we can satisfy the gradient relation in (x, y) -coordinates if we satisfy this relation on the orthogonal grid in (ξ, η) -coordinates. The gradient relation is *invariant under transformations*. This is in agreement with the fact that this relation can be satisfied regardless of the size and shape of the grid as we argued in Section 3.

A similar result holds for the divergence equation. Let $\nabla \cdot \mathbf{u} + \psi - f = 0$ be integrated over a 3-dimensional volume in (ξ, η) -coordinates² with integrand $(\nabla \cdot \mathbf{u} + \psi - f) d\xi d\eta$, then in Ω this becomes

$$(62) \quad \frac{1}{J} (\nabla \cdot \mathbf{u} + \psi - f) dx dy = 0 ,$$

which can be satisfied when $(\nabla \cdot \mathbf{u} + \psi - f) d\xi d\eta = 0$. So, also the divergence relation is invariant under transformations.

²We still assume unit distance in the ζ -direction and no dependence on ζ . See also remarks in Section 4.3

The constitutive relations are *not* invariant under transformations. Take for example, $\gamma = 1$ in the relation, then $\psi = \gamma\phi$ becomes

$$(63) \quad \frac{1}{J}\psi(\xi, \eta) = \phi(\xi, \eta),$$

which explicitly depends on the determinant of the Jacobian $J(\xi, \eta)$. Note that we can interpret this transformed equation to the untransformed equation with $\gamma(\xi, \eta) = J(\xi, \eta)$. Similarly, for the equation $\mathbf{u} = \mathbb{A}\mathbf{v}$ with $\mathbb{A} = \mathbb{I}$ we obtain

$$(64) \quad \begin{aligned} & \frac{1}{J} \left[\left(p \frac{\partial \Phi^x}{\partial \xi} + q \frac{\partial \Phi^x}{\partial \eta} \right) dy - \left(p \frac{\partial \Phi^y}{\partial \xi} + q \frac{\partial \Phi^y}{\partial \eta} \right) dx \right] \\ &= \frac{1}{J} \left[\left(u \frac{\partial \Phi^y}{\partial \eta} - v \frac{\partial \Phi^y}{\partial \xi} \right) dy - \left(-u \frac{\partial \Phi^x}{\partial \eta} + v \frac{\partial \Phi^x}{\partial \xi} \right) dx \right]. \end{aligned}$$

If we replace $dx = \frac{\partial \Phi^x}{\partial \xi} d\xi + \frac{\partial \Phi^x}{\partial \eta} d\eta$ and $dy = \frac{\partial \Phi^y}{\partial \xi} d\xi + \frac{\partial \Phi^y}{\partial \eta} d\eta$ in this constitutive relation, i.e. bringing the relation back from Ω to Ω_0 , then we obtain

$$\begin{aligned} -q d\xi + p d\eta &= \frac{1}{J} \left[u \frac{\partial \Phi^y}{\partial \eta} \frac{\partial \Phi^y}{\partial \xi} - v \frac{\partial \Phi^y}{\partial \xi} \frac{\partial \Phi^y}{\partial \xi} + u \frac{\partial \Phi^x}{\partial \eta} \frac{\partial \Phi^x}{\partial \xi} - v \frac{\partial \Phi^x}{\partial \xi} \frac{\partial \Phi^x}{\partial \xi} \right] d\xi + \\ & \frac{1}{J} \left[u \frac{\partial \Phi^y}{\partial \eta} \frac{\partial \Phi^y}{\partial \eta} - v \frac{\partial \Phi^y}{\partial \xi} \frac{\partial \Phi^y}{\partial \eta} + u \frac{\partial \Phi^x}{\partial \eta} \frac{\partial \Phi^x}{\partial \eta} - v \frac{\partial \Phi^x}{\partial \xi} \frac{\partial \Phi^x}{\partial \eta} \right] d\eta. \end{aligned}$$

in terms of the components p, q, u and v expressed in (ξ, η) -coordinates this states that

$$\begin{pmatrix} p \\ q \end{pmatrix} = \begin{pmatrix} \left(\frac{\partial \Phi^y}{\partial \eta} \right)^2 + \left(\frac{\partial \Phi^x}{\partial \eta} \right)^2 & -\frac{\partial \Phi^y}{\partial \xi} \frac{\partial \Phi^y}{\partial \eta} - \frac{\partial \Phi^x}{\partial \xi} \frac{\partial \Phi^x}{\partial \eta} \\ -\frac{\partial \Phi^y}{\partial \xi} \frac{\partial \Phi^y}{\partial \eta} - \frac{\partial \Phi^x}{\partial \xi} \frac{\partial \Phi^x}{\partial \eta} & \left(\frac{\partial \Phi^y}{\partial \xi} \right)^2 + \left(\frac{\partial \Phi^x}{\partial \xi} \right)^2 \end{pmatrix} \begin{pmatrix} u \\ v \end{pmatrix}.$$

So the isotropic relation in (x, y) -coordinates transforms to an anisotropic relation in (ξ, η) -coordinates. The matrix is clearly symmetric and its determinant is equation to J , so in order to have a positive definite tensor relating (p, q) and (u, v) , we need to have transformations which preserves the orientation.

7. RESULTS

In this section we want to illustrate the spectral mimetic least-squares method by means of a test problem. We consider the problem with $\mathbb{A} = \mathbb{I}$ and $\gamma = 1$,

$$-\nabla \cdot \nabla \phi + \phi = f$$

with

$$f(x, y) = (2\pi^2 + 1) \sin(\pi x) \sin(\pi y) \quad \text{and} \quad \phi = 0 \text{ along } \partial\Omega,$$

on the domain $\Omega = [-1, 1]^2$ with exact solution

$$\phi_{ex}(x, y) = \sin(\pi x) \sin(\pi y).$$

Although the use of $\mathbb{A} = \mathbb{I}$ and $\gamma = 1$ seems restrictive, the analysis in Section 6 revealed that the approximation on deformed grids is equivalent to the use of non-trivial \mathbb{A} and γ on orthogonal grids.

In Section 7.1 we compare the results obtained from the four-field functional (19) with the mimetic four-field functional (11). In Section 7.2 we investigate the use of different polynomial representations on dual elements. Finally, we will assess the performance of the mimetic least-squares formulation on highly deformed grids in Section 7.3.

The domain is divided in $K \times K$ elements. The solution is represented on the reference domain $(\xi, \eta) \in \Omega_{ref} = [-1, 1]^2$ and mapped onto the respective elements in (x, y) -coordinates using maps as discussed in Section 6. We will use the following polynomial

expansions for ϕ , ψ , \mathbf{v} and \mathbf{u} on the reference domain with $N = M$, see Section 4.2 and $\tilde{N} = \tilde{M}$, see Section 4.3

$$\begin{aligned}\phi^h(\xi, \eta) &= \sum_{i=0}^N \sum_{j=0}^N \phi_{i,j} \ell_i^0(\xi) \ell_j^0(\eta) \in \mathbb{P}^{N,N} \\ \mathbf{v}^h(\xi, \eta) &= \sum_{i=1}^N \sum_{j=0}^N u_{i,j} \ell_i^1(\xi) \ell_j^0(\eta) + \sum_{i=0}^N \sum_{j=1}^N v_{i,j} \ell_i^0(\xi) \ell_j^1(\eta) \in \mathbb{P}^{N-1,N} \times \mathbb{P}^{N,N-1}, \\ \mathbf{u}^h(\xi, \eta) &= \sum_{i=0}^{\tilde{N}} \sum_{j=1}^{\tilde{N}} p_{i,j} \tilde{\ell}_i^0(\xi) \tilde{\ell}_j^1(\eta) - \sum_{i=1}^{\tilde{N}} \sum_{j=0}^{\tilde{N}} q_{i,j} \tilde{\ell}_i^1(\xi) \tilde{\ell}_j^0(\eta) \in \mathbb{P}^{\tilde{N},\tilde{N}-1} \times \mathbb{P}^{\tilde{N}-1,\tilde{N}}, \\ \psi^h(\xi, \eta) &= \sum_{i=1}^{\tilde{N}} \sum_{j=1}^{\tilde{N}} \psi_{i,j} \tilde{\ell}_i^1(\xi) \tilde{\ell}_j^1(\eta) \in \mathbb{P}^{\tilde{N}-1,\tilde{N}-1},\end{aligned}$$

where N denotes the polynomial degree on the primal grid and \tilde{N} denotes the polynomial degree on the dual grid. In both cases the discrete degrees of freedom are the geometric cochains representing integral values of over the associated geometric objects. These polynomial spaces are compatible with the gradient on the primal grid and the divergence on the dual grid, see also [11].

From interpolation theory we know that for sufficiently smooth exact solution the expected rates of convergence are $\epsilon_\phi = O(h^{N+1})$, $\epsilon_{\mathbf{v}} = O(h^N)$, $\epsilon_{\mathbf{u}} = O(h^{\tilde{N}})$ and $\epsilon_\psi = O(h^{\tilde{N}-1})$.

With this polynomial reconstruction of the cochains, ϕ^h is globally C^0 , \mathbf{v}^h has tangential continuity between elements, \mathbf{u}^h has normal continuity and ψ^h is discontinuous between elements.

7.1. Least-squares and mimetic least-squares functional. We illustrate the difference between the standard least-squares formulation for the four-field system (9) based on the functional

$$(65) \quad \mathcal{J}(\mathbf{u}, \mathbf{v}, \phi, \psi; f) := \frac{1}{2} \left(\|\nabla \cdot \mathbf{u} + \psi - f\|_0^2 + \|\mathbf{v} + \nabla \phi\|_0^2 + \|\mathbb{A}^{-1/2} (\mathbf{u} + \mathbb{A}\mathbf{v})\|_0^2 + \|\gamma^{-1/2} (\psi - \gamma\phi)\|_0^2 \right),$$

and the mimetic least-squares formulation for the same problem based on the functional

$$(66) \quad \tilde{\mathcal{J}}(\mathbf{u}, \mathbf{v}, \phi, \psi; f) := \frac{1}{2} \left(\|\nabla \cdot \mathbf{u} + \psi - f\|_0^2 + \|\mathbf{v} + \nabla \phi\|_0^2 + \|\mathbb{A}^{-1/2} (\mathbf{u} + \mathbb{A}\nabla \phi)\|_0^2 + \|\gamma^{-1/2} (\nabla \cdot \mathbf{u} - \gamma\phi - f)\|_0^2 \right).$$

In Figure 5 h -convergence for ϕ and \mathbf{v} for the least-squares functionals (65) and (66) is shown for the case $N = \tilde{N}$. Only the mimetic least-squares formulations display optimal convergence with h -refinement of $O(h^{N+1})$ for ϕ and $O(h^N)$ for \mathbf{v} . In Figure 6 h -convergence on the dual complex for the variables \mathbf{u} and ψ is displayed. Both formulations show optimal convergence with h -refinement with $O(h^{\tilde{N}})$ for both \mathbf{u} and ψ . The black solid lines in these figures indicate the observed rate of convergence.

The main difference in both least-squares formulations is shown in Figure 7. On page 6 it was argued that the mimetic least-squares formulation is *not* equivalent to the least-squares formulation of the four-field problem (9). This is illustrated by the solid lines in Figure 7. In Figure 7a we see that the constraint $\nabla \times \mathbf{v} = \nabla \times \nabla \phi = 0$ is only *approximated*. For the case $N = 1$, the least-squares formulation based on (65) does not even converge.

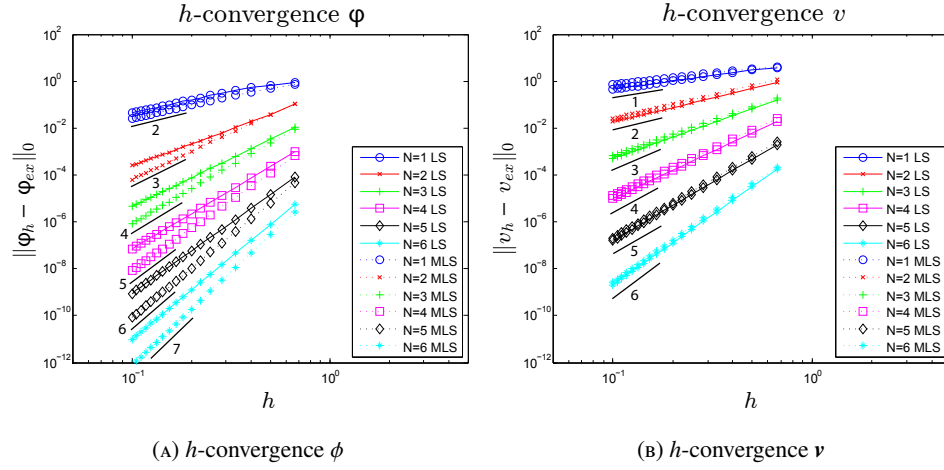


FIGURE 5. h -convergence for ϕ and v for various polynomial orders on a uniform orthogonal grid for the conventional least-squares formulation (solid lines) based on the functional (65) and the mimetic least-squares functional (dotted lines) based on the functional (66). The observed rate of convergence is indicated by the black slope lines.

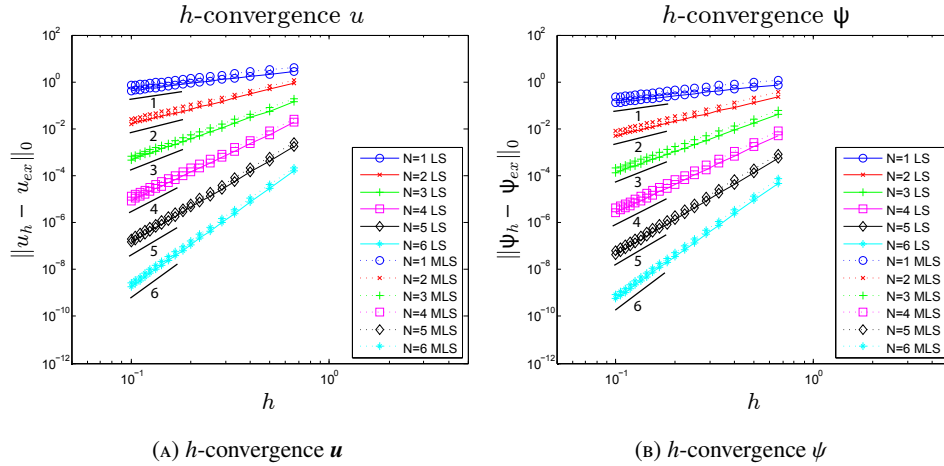


FIGURE 6. h -convergence for u and ψ for various polynomial orders on a uniform orthogonal grid for the conventional least-squares formulation (solid lines) based on the functional (65) and the mimetic least-squares functional (dotted lines) based on the functional (66). The observed rate of convergence is indicated by the black slope lines.

Figure 7b shows that the least-squares formulation based on the functional (65) only *approximates* the relation $\nabla \cdot \mathbf{u} + \psi = f$, while the least-squares formulation based on (66) satisfies this constraint up to machine accuracy.

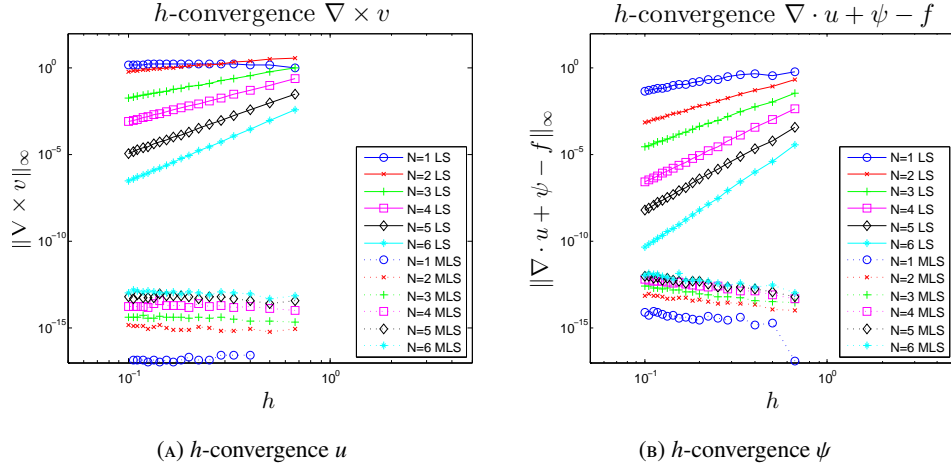


FIGURE 7. h -convergence for $\nabla \times v$ and $\nabla \cdot u + \psi - f$ in the ∞ -norm for various polynomial orders on a uniform orthogonal grid for the conventional least-squares formulation (solid lines) based on the functional (65) and the mimetic least-squares functional (dotted lines) based on the functional (66)

On page 6 it was argued that the error in the conservation laws is proportional to the error in the constitutive equations when the least-squares functions (65) is used

$$\int_{\Omega} (\nabla \cdot \mathbf{u}^h + \psi^h - f) \tilde{\psi}_h \, dx = \int_{\Omega} (\psi^h - \phi^h) \tilde{\psi}_h \, dx \quad \forall \tilde{\psi}.$$

For the specific choice $\tilde{\psi}^h = \nabla \cdot \mathbf{u}^h + \psi^h - f$ this gives

$$\begin{aligned} \|\nabla \cdot \mathbf{u}^h + \psi^h - f\|^2 &= \int_{\Omega} (\nabla \cdot \mathbf{u}^h + \psi^h - f)^2 \, dx \\ &= \int_{\Omega} (\psi^h - \phi^h) (\nabla \cdot \mathbf{u}^h + \psi^h - f) \, dx \\ &\leq \|\nabla \cdot \mathbf{u}^h + \psi^h - f\| \cdot \|\psi^h - \phi^h\|. \end{aligned}$$

This implies that

$$\|\nabla \cdot \mathbf{u}^h + \psi^h - f\| \leq \|\psi^h - \phi^h\|.$$

Similarly, we have that

$$\|\mathbf{v}^h - \nabla \phi^h\| \leq \|\mathbf{u}^h - \mathbf{v}^h\|.$$

These observations are corroborated in Figure 8, where in Figure 8a both $\|\mathbf{v}^h - \nabla \phi^h\|$ and $\|\mathbf{u}^h - \mathbf{v}^h\|$ are plotted. In Figure 8b $\|\nabla \cdot \mathbf{u}^h + \psi^h - f\|$ and $\|\psi^h - \phi^h\|$ are plotted for various polynomial order. The plots in Figure 8 confirm that the error in the approximated conservation relations is bounded by the error in constitutive relations.

7.2. Different polynomial representations on dual elements. In Remarks 1 and 2 it was pointed out that for a mimetic least-squares formulation it is *not* necessary to have a strict one-to-one relation between dual variables. In Section 7.1 results were presented on the same grid, i.e. $N = \tilde{N}$, which violates this one-to-one correspondence. In this section we will show that we can use different polynomial degrees on dual elements. In Figures 9, 10 and 11 results are presented for the case $N = \tilde{N} + 1$, which also violates strict duality. All

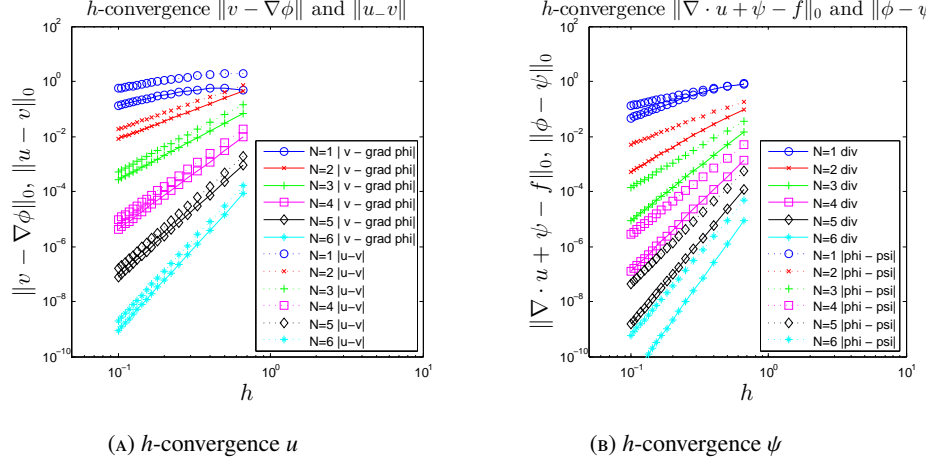


FIGURE 8. h -convergence for (A) $\mathbf{v} - \nabla\phi$ (solid line) and $\|\mathbf{u} - \mathbf{v}\|$ (dotted line), and (B) $\nabla \cdot \mathbf{u} + \psi - f$ (solid line) and $\|\phi - \psi\|$ (dotted line) in the L^2 -norm for various polynomial orders on a uniform orthogonal grid for the conventional least-squares formulation based on the functional (65)

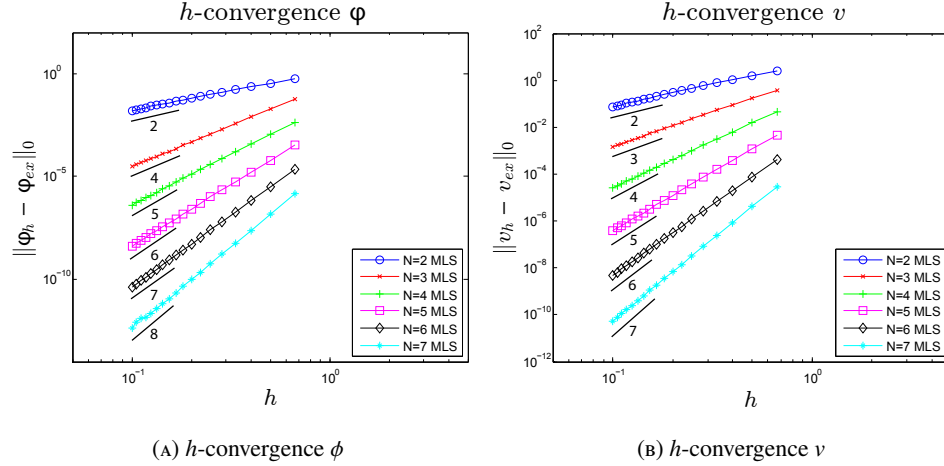


FIGURE 9. h -convergence for ϕ and v for various polynomial orders on a uniform orthogonal grid for the mimetic least-squares functional based on the functional (66) for the case $N = \tilde{N} + 1$. The observed rate of convergence is indicated by the black slope lines.

variables converge optimally with h -refinement as shown in Figures 9 and 10, except for ϕ when $N = 2$ and $\tilde{N} = 1$ where the observed rate of convergence is one order less than expected from interpolation theory. The conservation laws are still satisfied up to machine precision as shown in Figure 11, which was to be expected since the conservation laws are represented on one mesh only and are completely insensitive to the representation of the dual variables.

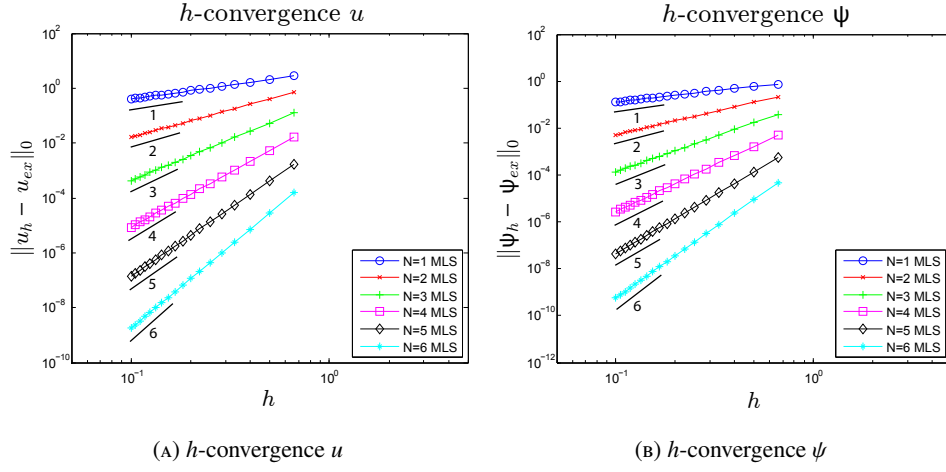


FIGURE 10. h -convergence for u and ψ for various polynomial orders on a uniform orthogonal grid for the mimetic least-squares functional based on the functional (66) for the case $N = \tilde{N} + 1$. The observed rate of convergence is indicated by the black slope lines.

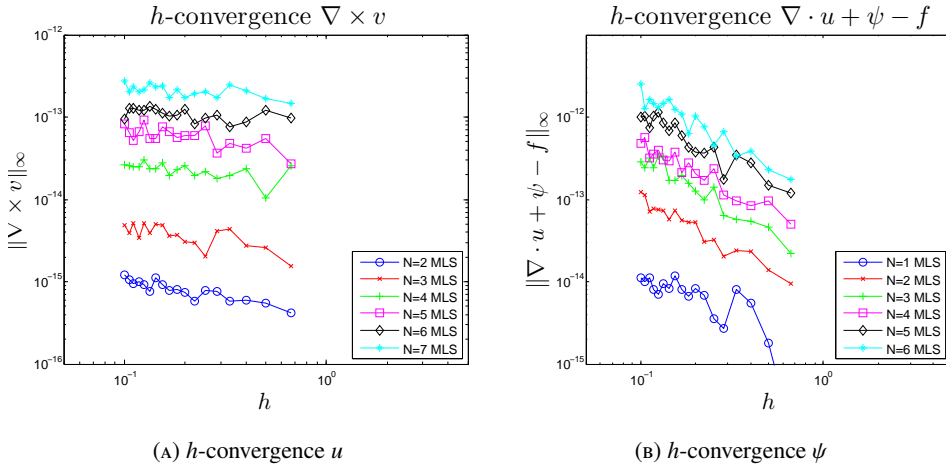


FIGURE 11. h -convergence for $\nabla \times v$ and $\nabla \cdot u + \psi - f$ for various polynomial orders on a uniform orthogonal grid for the mimetic least-squares functional based on the functional (66) for the case $N = \tilde{N} + 1$.

In Figures 12, 13 and 14 results are presented for the case $N = \tilde{N} - 1$. In this particular case the polynomial expansions for ϕ^h and ψ^h have the same polynomial degree and therefore strict duality for these variables hold. All variables converge optimally with h -refinement as shown in Figures 9 and 10. The conservation laws are still satisfied up to machine precision as shown in Figure 11.

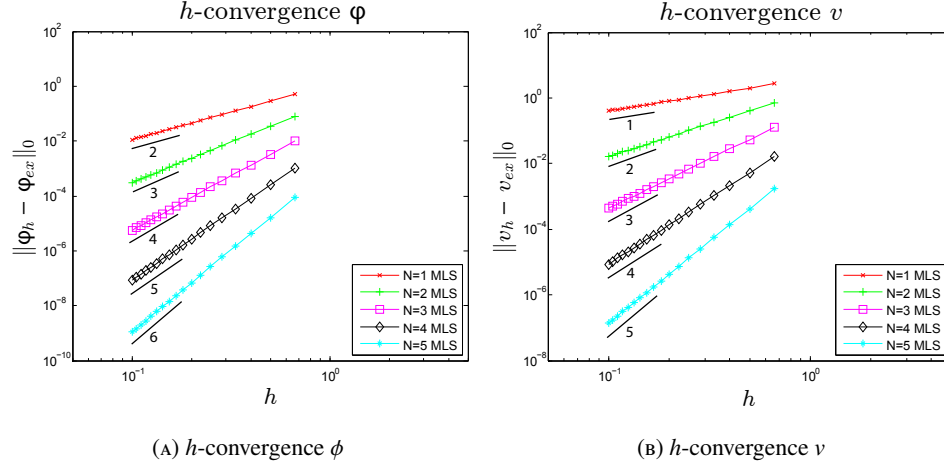


FIGURE 12. h -convergence for ϕ and v for various polynomial orders on a uniform orthogonal grid for the mimetic least-squares functional based on the functional (66) for the case $N = \tilde{N} - 1$. The observed rate of convergence is indicated by the black slope lines.

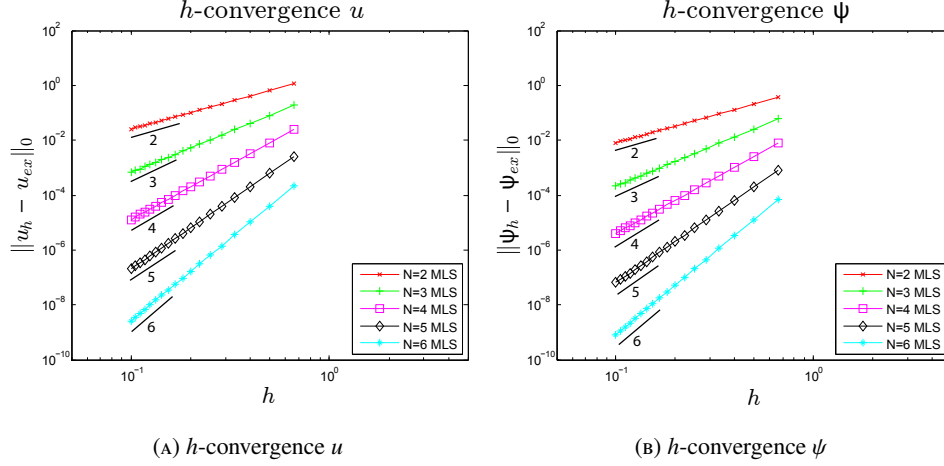


FIGURE 13. h -convergence for u and ψ for various polynomial orders on a uniform orthogonal grid for the mimetic least-squares functional based on the functional (66) for the case $N = \tilde{N} - 1$. The observed rate of convergence is indicated by the black slope lines.

The fact that we can use different polynomial approximations for the primal and dual variables and still obtain optimal convergence rates is a direct consequence of Proposition 2, Theorem 2 and Corollary 1, i.e. the fact that we have a conforming discrete representation which satisfies the DeRham sequence.

7.3. Mimetic least-squares on deformed grids. The previous results were all obtained on uniform orthogonal grids. The performance of the method on more general grids is

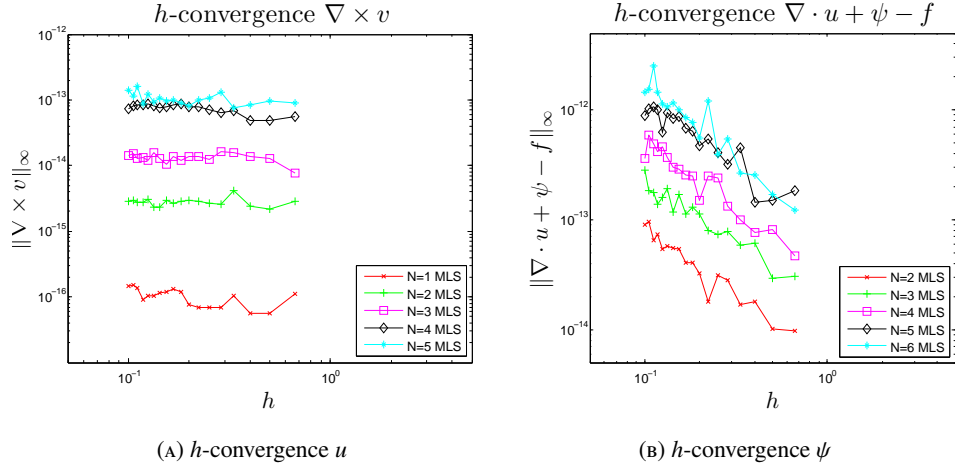


FIGURE 14. h -convergence for $\nabla \times v$ and $\nabla \cdot u + \psi - f$ for various polynomial orders on a uniform orthogonal grid for the mimetic least-squares functional based on the functional (66) for the case $N = \tilde{N} - 1$.

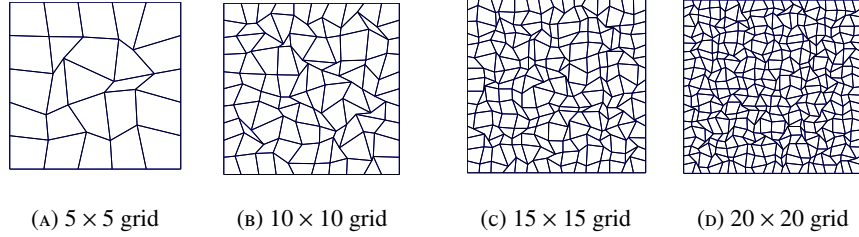


FIGURE 15. Several randomly perturbed grids, where the grid points are perturbed by a uniform distribution $[-h/2, h/2]$.

presented in this section. The grids that were used in these computations are the randomly perturbed grids, some of which shown in Figure 15. These grids are obtained by randomly perturbing the grid points of the uniform grid by adding an offset of $[-h/2, h/2]$ in both the x - and y -component. These grids contain degenerate cubes like triangles and even non-convex quadrilaterals.

Figures 16 and 17 show the convergence of the primal and the dual variables, respectively. As emphasized in Sections 3 and 6 the conservation laws are insensitive to the particular size and shape of the grid, which is illustrated in Figure 18. Both the gradient relation and the divergence equation are still satisfied up to machine precision.

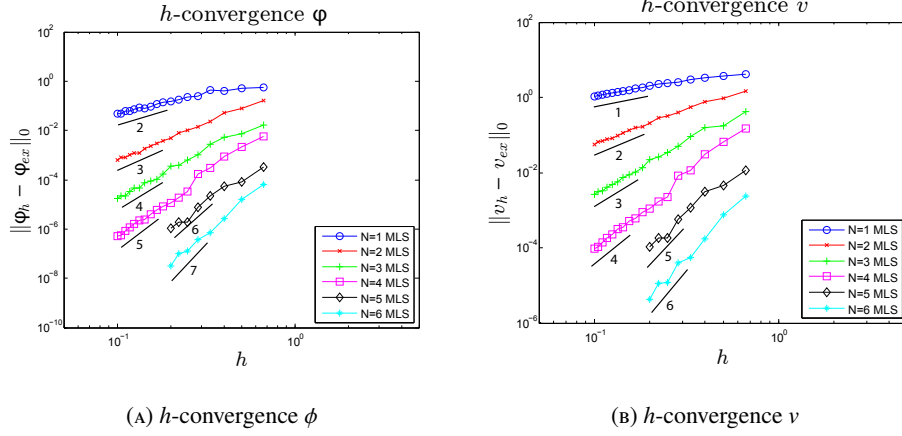


FIGURE 16. h -convergence for ϕ and v for various polynomial orders on the randomly perturbed grids shown in Figure 15 for $N_p = N_d$. The optimal rate of convergence is indicated by the black slope lines

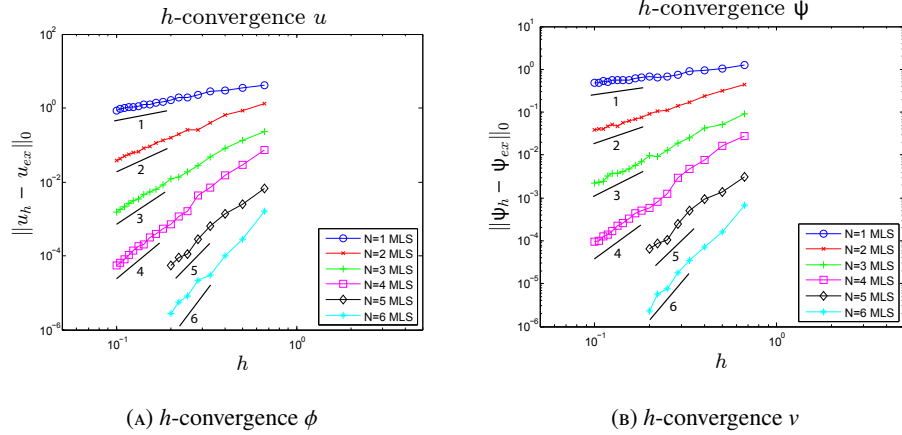


FIGURE 17. h -convergence for u and ψ for various polynomial orders on the randomly perturbed grids shown in Figure 15 for $N_p = N_d$. The optimal rate of convergence is indicated by the black slope lines

8. CONCLUSIONS

In this paper a spectral mimetic least-squares formulation is presented for reaction-diffusion problems. Topological operations like the gradient, curl and divergence can be satisfied up to machine precision in this formulation. We conclude that two requirements are necessary for a mimetic least-squares formulation:

- (1) The discrete space should allow for a discrete representation for the topological operators, see Section 4;
- (2) The least-squares functional should decouple the topological relations from the metric-dependent relations, see page 6.

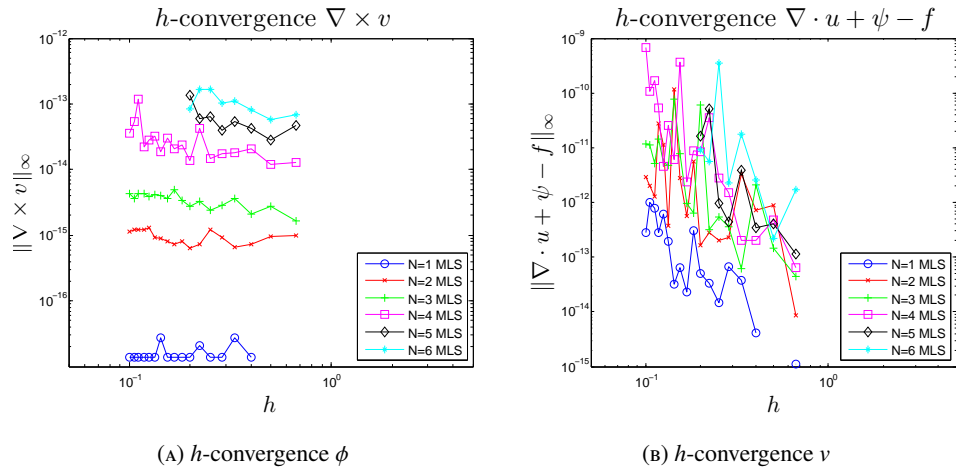


FIGURE 18. h -convergence for $\nabla \times v$ and $\nabla \cdot u + \psi - f$ in the ∞ -norm for various polynomial orders on the randomly perturbed grids shown in Figure 15 for $N_p = N_d$. The optimal rate of convergence is indicated by the black slope lines

The mimetic least-squares method still leads to a positive definite system. We do not need to satisfy an inf-sup condition. The use of standard C^0 -elements needs to be abandoned in favor of basis functions which preserve the geometric degrees of freedom.

These conclusions are confirmed by numerical results presented in Section 7.

REFERENCES

- [1] D. Arnold, R. Falk, and R. Winther. Finite element exterior calculus, homological techniques, and applications. *Acta Numerica*, 15:1–155, 2006.
- [2] P. Bochev and M. Gunzburger. On least-squares finite element methods for the Poisson equation and their connection to the Dirichlet and Kelvin principles. *SIAM Journal on Numerical Analysis*, 43(1):340–362, 2006.
- [3] P. Bochev and M. Gunzburger. A locally conservative least-squares method for Darcy flows. *Commun. Numer. Meth. Engng.*, 24:97–110, 2008.
- [4] P. Bochev and M. Gunzburger. *Least-squares finite element methods*. Springer, 2009.
- [5] P. Bochev and J. Hyman. Principles of mimetic discretizations of differential operators. In R. N. D. Arnold, P. Bochev and M. Shashkov, editors, *Compatible Spatial Discretizations*, volume 42 of *The IMA volumes in Mathematics and its Applications*, pages 89–119. Springer Verlag, 2006.
- [6] A. Bossavit. Computational electromagnetism and geometry. *Journal of the Japanese Society of Applied Electromagnetics and Mechanics*, 7, 8:150–9 (no 1), 294–301 (no 2), 401–408 (no 3), 102–109 (no 4), 203–209 (no 5), 372–377 (no 6), 1999, 2000.
- [7] J. H. Bramble, R. D. Lazarov, and J. E. Pasciak. Least-squares for second-order elliptic problems. *Computer Methods in Applied Mechanics and Engineering*, 152(1-2):195 – 210, 1998. Containing papers presented at the Symposium on Advances in Computational Mechanics.
- [8] S. S. Cairns. *Introductory topology*. Ronald Press, New York, 1961.

- [9] G. F. Carey and A. I. Pehlivanov. Local error estimation and adaptive remeshing scheme for least-squares mixed finite elements. *Computer Methods in Applied Mechanics and Engineering*, 150(1-4):125 – 131, 1997. Symposium on Advances in Computational Mechanics.
- [10] C. Chang and J. Nelson. Least-squares finite element method for the Stokes problem with zero residual of mass conservation. *SIAM Journal of Numerical Analysis*, 34:480–489, 1997.
- [11] L. Demkowicz. Polynomial exact sequences and projection-based interpolation with application to Maxwell equations. In D. Boffi, L. Demkowicz, R. Falk, F. Brezzi, R. Durán, and M. Fortin, editors, *Mixed Finite Elements, Compatibility Conditions, and Applications*, pages 101 – 158. Springer, 2008.
- [12] M. Desbrun, A. Hirani, M. Leok, and J. Marsden. Discrete Exterior Calculus. *Arxiv preprint math/0508341*, 2005.
- [13] M. Gerritsma. Edge functions for spectral element methods. In J. Hesthaven and E. Rønquist, editors, *Spectral and High Order Methods for Partial Differential Equations*, volume 76 of *Springer Lecture Notes in Computational Science and Engineering*, pages 199–208, 2011.
- [14] J. Heys, E. Lee, T. Manteuffel, and S. McCormick. On mass-conserving least-squares methods. *SIAM Journal on Scientific Computing*, 28:1675–1693, 2006.
- [15] J. Heys, E. Lee, T. Manteuffel, and S. McCormick. An alternative least-squares formulation of the Navier-Stokes equations with improved mass conservation. *Journal of Computational Physics*, 226:994–1006, 2007.
- [16] R. Hiptmair. Discrete Hodge operators. *Numerische Mathematik*, 90(2):265–289, 2001.
- [17] J. Hyman, J. Morel, M. Shashkov, and S. Steinberg. Mimetic finite difference methods for diffusion equations. *Computational Geosciences*, 6(3-4):333–352, 2002.
- [18] J. Hyman and S. Steinberg. The convergence of mimetic methods for rough grids. *Computers and Mathematics with applications*, 47(10-11):1565–1610, 2004.
- [19] J. M. Hyman and J. C. Scovel. Deriving mimetic difference approximations to differential operators using algebraic topology. Technical report, Los Alamos National Laboratory, 1990.
- [20] J. Kreeft and M. Gerritsma. Mixed mimetic spectral element method for Stokes flow: A pointwise divergence-free solution. *Journal of Computational Physics*, 240:284–309, 2013.
- [21] J. Kreeft, A. Palha, and M. Gerritsma. Mimetic framework on curvilinear quadrilaterals of arbitrary order. *arXiv:1111.4304*, 2011.
- [22] K. Lipnikov, G. Manzini, and M. Shashkov. Mimetic finite difference method. *Journal of Computational Physics*, 254:1163–1227, 2014.
- [23] A. Palha, P. Rebelo, R. Hiemstra, J. Kreeft, and M. Gerritsma. Physics-compatible discretization techniques on single and dual grids, with application to the Poisson equation for volume forms. *Journal of Computational Physics*, 257:1394–1422, 2014.
- [24] B. Perot. Discrete Conservation Properties of Unstructured Mesh Schemes. *Annual Review of Fluid Mechanics*, 43(1).
- [25] M. Proot and M. Gerritsma. Mass- and momentum conservation of the least-squares spectral element method for the Stokes problem. *Journal of Scientific Computing*, 27:389–401, 2006.

- [26] F. Rapetti and A. Bossavit. Geometrical localisation of the degrees of freedom for Whitney elements of higher order. *Science, Measurement Technology, IET*, 1(1):63–66, January 2007.
- [27] P. Raviart and J. Thomas. A mixed finite element method for 2nd order elliptic problems. *Mathematical Aspects of the Finite Element Method, Lecture Notes in Mathematics*, 606:292–315, 1977.
- [28] N. Robidoux and S. Steinberg. A discrete vector calculus in tensor grids. *Computational Methods in Applied Mathematics*, 1:1–44, 2011.

SANDIA NATIONAL LABORATORIES,
COMPUTATIONAL MATHEMATICS, MAIL STOP 1320, ALBUQUERQUE, NM 87185, USA

DELFT UNIVERSITY OF TECHNOLOGY, FACULTY OF AEROSPACE ENGINEERING,
KLUYVERWEG 2, 2629 HT DELFT, THE NETHERLANDS.
E-mail address: pbboche@sandia.gov, M.I.Gerritsma@TUDelft.nl